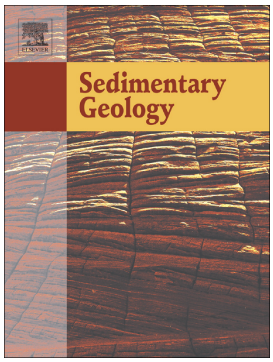

The origin of clay-coated sand grains and sediment heterogeneity in tidal flats

Luke J. Wooldridge, Richard H. Worden, Joshua Griffiths, James E.P. Utley, Anu Thompson

PII: S0037-0738(18)30155-6
DOI: doi:10.1016/j.sedgeo.2018.06.004
Reference: SEDGEO 5358

To appear in: *Sedimentary Geology*

Received date: 29 January 2018
Revised date: 29 May 2018
Accepted date: 12 June 2018

Please cite this article as: Luke J. Wooldridge, Richard H. Worden, Joshua Griffiths, James E.P. Utley, Anu Thompson , The origin of clay-coated sand grains and sediment heterogeneity in tidal flats. Sedgeo (2018), doi:10.1016/j.sedgeo.2018.06.004

The origin of clay-coated sand grains and sediment heterogeneity in tidal flats

LUKE J. WOOLDRIDGE*, RICHARD H. WORDEN, JOSHUA GRIFFITHS, JAMES E.P. UTLEY, ANU THOMPSON

School of Environmental Sciences, University of Liverpool, Liverpool L69 3GP, U.K.

Corresponding authors (e-mail: luke.wooldridge@liv.ac.uk)

Abstract

The presence and distribution of clay minerals attached to grain surfaces as coats (also known as rims) are of great interest because they affect petroleum reservoir quality via the inhibition of the porosity-occluding quartz cement during prolonged burial and heating. Being able to predict the distribution of clay-coated sand grains in petroleum reservoirs is thus important to help find and exploit anomalously high porosity sandstones deep in sedimentary basins. The few studies focused on the distribution of clay coats in marginal marine sediments derive from surface sediment-based data sets, with limited emphasis placed on the preservation of the surface trends in sediment undergoing eodiagenesis in the near-surface environments. The post-depositional processes of bioturbation (sediment homogenisation) and infiltration of clay into sand-grade sediment have been widely invoked as potential mechanisms that produce clay coats in modern sands and ancient sandstones. However, the potential for such processes to alter surface trends and govern clay-coat distribution in the subsurface remains unconstrained. In this study, we report the development of a novel, quantitative model of clay-coat coverage in order to identify the controlling mechanisms that govern clay-coat distributions. This study has focused on surface and near-surface sediments in the Saltcoats tidal flat deposits of the Ravenglass Estuary, UK. This

unique bio-sedimentary study involved geomorphic mapping, core logging, a range of scanning electron microscopy techniques, and quantification of grain-size, clay fraction content, biofilm abundance (total carbohydrate and biomarker analysis), clay-coat coverage, and clay-coat mineralogy. In this study, against established convention, we demonstrate that infiltration and bioturbation do not significantly affect clay-coat grain coverage in near-surface sediments. Instead, we show that the extent, distribution, and mineralogy of clay coats in near-surface sediment are governed by the surface-based hydrological segregation of the clay mineral assemblage and biological clay-coat formation.

Keywords: clay coated sand grains, clay mineralogy, reservoir quality, modern analogue, biofilms, sediment heterogeneity

1. Introduction

One of the most widely reported origins for the preservation of anomalously high porosity deep in sedimentary basins is the presence of clay coats (rims) on sand-grain surfaces (Ehrenberg, 1993; Worden and Morad, 2000; Bloch et al., 2002; Ajdukiewicz and Larese, 2012). Chlorite- and illite-coated sand grains have been shown to inhibit the growth of the otherwise ubiquitous, porosity-occluding quartz cement at depth (Billault et al., 2003; Lander et al., 2008; Ajdukiewicz and Larese, 2012). Illite tends to cause permeability problems as it forms a mesh of pore-filling fibres and so is not necessarily a benefit to sandstone reservoir quality (Worden and Morad, 2003). Chlorite tends to develop as thin coats on sand grains that do not block pore throats (Ehrenberg, 1993; Dowey et al., 2012); chlorite is thus prized as a benefit to sandstone reservoir quality as it can lead to anomalously high porosity deep in sedimentary basins by preventing quartz cementation (Worden et al., 2018).

Diagenetic processes (compaction, cementation, and mineral dissolution) experienced by deeply-buried sandstones (> 3 km) typically prevent the preservation of economically viable porosity (Worden and Morad, 2000; Worden and Burley, 2003). The need to understand the origin of anomalously high porosity in deeply-buried sandstones has driven significant research into the prediction of clay-coated grains (Wilson, 1992; Bloch et al., 2002; Dowey et al., 2012; Saïag et al., 2016). Many recent attempts to constrain a predictive capability have focused on producing modern analogue models from surface based analyses (Dowey, 2013; Dowey et al., 2017; Wooldridge et al., 2017a; Wooldridge et al., 2017b), since clay coats within surface sediments potentially represent precursor coats to those found in some deeply buried sandstones (Needham et al., 2005). However, limited focus has been placed on the preservation of identified trends into near-surface sedimentary deposits.

There has been only a small amount of research reported on the potential role of infiltration and bioturbation in controlling the formation and distribution of clay-coated sand grains in near-surface sediments (Matlack et al., 1989; Wilson, 1992; Needham et al., 2005). Despite the small number of studies that have tried to examine the links between infiltration and bioturbation to clay-coated sand grains, these processes remain widely cited in both modern (Dowey, 2013; Dowey et al., 2017) and ancient marginal marine sediments (Moraes and De Ros, 1992; Bloch et al., 2002; Gier et al., 2008). This paper aims to constrain, via a modern analogue, the both the distribution of clay coated sand grains and the role played by post depositional processes on controlling the characteristics of clay-coated sand grains.

Tidal flats occur on a wide range of coastlines (with tidal ranges from less than 1 m to >15 m) and represent an important depositional component of both estuarine and deltaic systems (Semeniuk, 2005; Flemming, 2012). Sandstones that were originally deposited in tidal flat environments are a component that is widely reported in marginal-marine petroleum reservoir systems and form reservoir facies from a number of well-characterised systems: e.g., the Cretaceous Sacha Field, Oriente Basin, Ecuador (Higgs et al., 2002), the Lower Jurassic Beatrice Field, North Sea (Stevens, 1991), and the Jurassic Heather Field, North Sea (Glasmann et al., 1989).

The multi-scale heterogeneity of tidal sandstones represents a challenge for reservoir characterisation in terms of constraining modelling parameters, and in planning oil and gas field developments (Martinius et al., 2005). Previous work on the characterisation of tidal flat sediments has focused on classifying: morphology (Yang et al., 2005; Flemming, 2012), sedimentary textures (Chang and Choi, 2001; Chakrabarti, 2005; Flemming, 2012), the effect of hydraulic dynamics on grain size distribution (Chang and Choi, 2001; Brockamp and Zuther, 2004; Yang et al., 2005), sediment mineralogy, and sediment clay fraction distribution (< 2 μm) (Brockamp and Clauer, 2012). However, the biological aspect of tidal flat sedimentary environments remains relatively poorly defined and largely un-quantified (Jones, 2017).

Tidal flat sediments are composed of non-cohesive sand, cohesive mud, and the excretions of sticky, cohesive extracellular polymeric substances (EPS) by colonizing biological organisms (Malarkey et al., 2015; Jones, 2017). Biological organisms, in particular those that develop biofilms (molecular networks of sticky EPS) among sediment grains (Hoagland et al., 1993; Stal, 2003; Garwood et al.,

2015), have been shown to play a fundamental role on the dynamics and characteristics of estuarine tidal flat sediments (Stal, 2003; Garwood et al., 2015; Schindler et al., 2015; Wooldridge et al., 2017a).

Biofilms are produced via the secretion of EPS (adhesive mucilage) by sediment-inhabiting microphytobenthic (MPB) biological communities that are composed of diatoms, euglenids, crysophyceans, dinoflagelates, cyanobacteria, and photosynthetic bacteria (Jesus et al., 2009). Sediment colonising benthic diatoms account for > 95 % of all benthic organisms in the tidal flat settings of western Europe (Underwood and Paterson, 1993) and therefore are the principal focus of this work. Marginal marine biofilms in sediments have been shown to increase sediment cohesion which in turn influences (i) tidal flat erosion rates (Vos et al., 1988; Hoagland et al., 1993), (ii) grain size heterogeneity (Garwood et al., 2015), (iii) tidal flat geomorphology (Stal, 2010), and (iv) bedform stability (Malarkey et al., 2015; Schindler et al., 2015). Note that the origin and characterisation of the sedimentological aspects of biofilms have been the subject of earlier studies (Hoagland et al., 1993; Stal, 2003; Jones, 2017; Wooldridge et al., 2017a).

This work documents the heterogeneity of a tidal flat by characterising the surface and near-surface distribution trends in grain size, grain sorting, clay fraction percentage (< 2 μm), biological populations (macro- and micro-organism), biofilm abundance, and clay-coat coverage. Since sampling was undertaken at high resolution, the study permitted the quantification of post-depositional processes, such as infiltration of fine grained material (clay) into a sand-dominated matrix and bioturbation on the formation of clay-coated sand grains. By focussing on the Saltcoats tidal flat in the Ravenglass Estuary, UK (Fig. 1), we will addresses the following specific questions:

1. What are the sedimentological and biological characteristics of a tidal flat sedimentary package?
2. What are the textural characteristics of clay-coated sand grains in a tidal flat sedimentary package?
3. How are clay-coated sand grains distributed in a tidal flat sedimentary package?
4. Is there a difference in the extent of clay-coats on sand grains at the sediment surface and sand grains in the near-surface at a depth of 1 m below the surface?
5. What controls the distribution of clay-coated sand grains in near-surface sediment?

2. Study site

This study focused on the Saltcoats siliciclastic tidal flat, in the Ravenglass Estuary, northwest England, UK (Wooldridge et al., 2017b). The 5.6 km^2 area Ravenglass Estuary is a shallow, macro-tidal, mixed-energy system that is dominated by tidal flats (Lloyd et al., 2013; Wooldridge et al., 2017b). Saltcoats represents the largest tidal flat (~ 0.35 km^2) located at the confluence of the River Irt and River Mite arms of the estuary (Fig. 1). Topographically the tidal flat consists of a fringing area with established saltmarsh vegetation around an intertidal area that sits at 3.5 m elevation O.D.. The estuary experiences a maximum 7.55 m spring tidal range (Lloyd et al., 2013).

3. Materials and Methods

The work focused on both surface and near-surface sediments with results initially reported separately for both. To allow comparison of this modern dataset to ancient sandstones originally deposited in the same environmental conditions,

trends in sedimentological and biological distributions have been segregated into tidal flat depositional environments and corresponding core (near-surface) sedimentary facies. Surface depositional environments and bedforms were mapped in the field with samples collected in a grid system and plotted using the interpolation function in ArcGIS (https://www.arcgis.com). A Pearson's correlation coefficient was used to test the statistical significance between all sedimentary and biological variables.

3.1. Surface data sets

The intensity of bioturbation by macro-organisms was quantified by counting lugworm (*Arenicola marina*) faecal cast density, recorded in the field in 1 m^2 quadrats at 140 sites on the tidal flat (Fig. 1C).

Detailed surface sedimentary data were collected from 22 samples including: the exact proportions of the clay fraction (< 2 μm), grain sizes, and sorting values. Quantitative sediment grain size and sorting analysis was undertaken via laser granulometry using a Beckman Coulter LS200, with values presented in the modified geometric graphical measures (Folk and Ward, 1957). The clay-fraction (< 2 μm) of the sediment, not well characterised using laser granulometry, was calculated from representative homogenised sediment sub-samples following the methodology outlined in Wooldridge et al. (2017b).

Eight polished thin sections were prepared (Fig. 1C), covering the range of depositional-sub-environments.

3.2. Near-surface data sets

The five-core transect spans about 500 m length it is approximately normal to the shoreline and encompasses the range of depositional environments from mud flat (core A), upper mixed flat (core B), lower mixed flat (core C), tidal creek point-bar

(core D), and sand flat (core E) (Fig. 1B). Images of surface environmental conditions are presented in Figure 2.

The five 1-m cores (50 mm diameter) were collected using a jack-hammer window sampler. Core B (mixed tidal flat, Fig. 1B) was collected in duplicate with the second core used for biological analyses. All cores were logged for grain size and sorting (determined in the laboratory using a hand-lens), primary sedimentary structures and bioturbation intensity (Taylor and Goldring, 1993). In total, 46 sediment subsamples were taken from the five cores at approximately uniform spacing but also ensuring collection of samples from each sediment facies; sampling points are marked in Figure 3. Polished thin sections of impregnated grain-mounts were made from the 46 subsamples. Laser granulometry analyses of grain size and sorting, plus clay fraction analyses, were undertaken at the same points sampled for thin section preparation.

3.3. Classification of samples: depositional environments, facies, and mineralogy

Samples were classified by lab-derived sand percentages into sand flat (> 90 % sand), mixed-(sand-mud) flat (50-90 % sand), and mud flat (15-50 % sand) (Brockamp and Zuther, 2004). The tidal flat classification (sand-mud ratio) was applied to define surface environments (accompanied by geomorphological mapping of the tidal flats) and the near-surface deposits (accompanied by lithofacies identification).

The sedimentary facies identified from cores have also been grouped into characteristic facies associations (e.g., by texture, sedimentary structures, bioturbation intensity, and diagnostic features) which are diagnostic of specific depositional environments (i.e., mud-, mixed-, and sand flats) in tidal flat environments. The lithofacies scheme was used to cross-check the validity of the

sand-mud ratio classification in assigning near-surface samples into the correct tidal flat depositional environment. The use of sand-mud ratios as determined by laser granulometry, instead of descriptive facies classifications, allowed direct quantitative comparison of the surface and near-surface datasets.

Sediment mineralogy was quantified using automated scanning electron microscope-energy dispersive spectrometry (SEM-EDS) techniques with an FEI-QEMSCAN® (Armitage et al., 2010; Wooldridge et al., 2017b). The approach enabled *in situ* imaging of thin sections as well as quantification of sediment mineralogy. The SEM-EDS analysis step-size was 1 µm to ensure that the fine fraction was analysed in unison with the framework grains, thus enabling identification of both the micron-scale morphology and mineralogical composition of sediment samples. Data are here presented as a combination of a backscatter secondary electron image, and quantitative mineralogical content images of bulk-sediment and clay fraction components with values reported in image-area percentages.

3.4. Clay-coat coverage and mineralogy

Polished thin sections were prepared from both surface (approximately 2 cm depth) and near-surface sediment (as deep as 1 m). Thin sections were analysed by scanning electron microscopy (SEM) in backscattered electron mode with SEM-EDS undertaken to quantify clay-coat morphology and mineralogy. Grain-mount stubs of loose sediment were also analysed for clay-coat morphology via SEM using a Hitachi TM3000 Tabletop Microscope equipped with a secondary X-ray detector.

Each thin section sample had 15 SEM images taken to create a micron-scale representative image of the sediment. Clay-coat quantification was undertaken

using SEM images in the Petrog statistical software (Wooldridge et al., 2017a). The method involved calculating the total perimeter of a grain and the length of the grain that is covered by attached clay coats (i.e., independent of clay-coat thickness) for 50 sand grains per sample, which produced a dataset of > 2600 analysed clay-coated sand grains. The method carries ± 1.7 % error with average percentage clay-coat values reported (Wooldridge et al., 2017a).

The mineralogical quantification of the clay-coated sand grains (clay coats and framework grains) was undertaken in SEM-EDS (see previous) on surface and near-surface samples to permit the *in situ* micron-scale mineralogical characterisation of the clay-coated sand grains.

3.5. Determination of biofilm sediment abundance (surface sediments)

The distribution of surface sediment biofilm abundance was mapped by measuring the abundance of the biomarker chlorophyll-a (Stal, 2003; Jiménez et al., 2015). Eighteen surface sediment samples were collected on a single day within 1 hour of low tide (Fig. 1C). The surface material was collected in sterilized foil, initially stored over ice during collection, and then stored at -18 °C during transport and then preserved at -80 °C when back at Liverpool University within 4 hours of collection. Chlorophyll-a analyses were undertaken following the methodology previously outlined in Wooldridge et al. (2017a); analysis of replicates revealed a relative error of <1%.*3.6. Determination of biofilm sediment abundance (near-surface)*

The chlorophyll-a biomarker approach to determine the amount of sediment biofilm material only works for the top approximately 4 mm of sediment, reflecting the present-day environmental niche of the diatoms (MPB) that produce biofilms (Stal, 2003). To assess whether surface trends of biofilm abundance are preserved into the near-surface, the total carbohydrate (biofilm) sediment component was calculated via the phenol-sulphuric assay (Underwood et al., 1995). The phenol–sulphuric assay is a colorimetric method widely used to determine the total sediment carbohydrate concentration (including mono-, di-,

oligo-, and polysaccharide) (Underwood and Paterson, 1993; Underwood et al., 1995; De Winder et al., 1999).

Samples were collected from the duplicate (< 0.5 m distance apart) core of B, B1 (Fig. 1B), with samples collected from each encountered facies, which encompassed sediment deposited originally in mud-, mixed-, and sand- tidal flat depositional environments. Sample collection was undertaken immediately upon extraction of the core. Samples were collected in sterilized foil, stored on ice during collection, placed in a freezer at -18°C for transport (4 hours) back to Liverpool University and then preserved at -80 °C.

Analytical-grade glucose standard was purchased from Sigma-Aldrich. Calibration standards in the range of 5 to 100 µg /mL (in the range 30-550 µM glucose) were prepared from a stock solution of glucose (0.1 mg/mL in water) in 25ml volumetric flasks. A total of 400 µl of each glucose standard and pure distilled water (performing as a blank) were added to a series of vials and 400 µl volumes of 5 % phenol (w/v), were then added to each of the vials followed by vortex mixing. Exactly 2 ml of concentrated, analytical grade sulphuric acid was added rapidly to each vial, vortex-mixed and the resulting vials incubated for 35 min. at room temperature. The absorbance of each calibration standard solution was then measured on a Jenway 7315 UV/VIS spectrophotometer at 490 nm and 570 nm against the blank.

Samples collected in the field were treated identically to the standards. Typically, 0.2 mg of freeze-dried sediment from each sample was weighed, with 400 µl of distilled milli-q water and 400 µl of 5 % phenol (w/v) added to each sample-extract and incubated at room temperature for 1 hour. Exactly 2 ml of concentrated sulphuric acid was added rapidly in a direct stream of acid against

the liquid surface. The extracts were transferred and centrifuged at 10,000 rpm for 1 min. The absorbance was measured at 490 nm and 570 nm via a Jenway 7315 UV/VIS spectrophotometer. Method blanks (no sediment added) were treated in the same manner as the samples.

A standard curve (absorption against glucose concentration) was generated to allow the calculation of the concentration of carbohydrate in each sample. The concentration of carbohydrate in the sample was calculated using the following formula: Concentration of glucose in samples (µg/g) = [concentration in µg/ml] /slope x weight of dried sediment extracted x dilution (ml).

4. Results

The results are presented in the four themes of the study: (i) sediment heterogeneity, (ii) biological content (macro-and micro-organism distribution and sediment biofilm abundance), (iii) clay coat coverage variability, and (iv) clay coat mineralogy. The results of each theme are further separated into surface and near-surface data sets.

4.1. Sediment heterogeneity: depositional environment, grain size, grain sorting, clay fraction content, and sediment mineralogy

Surface sediment characteristics

The Saltcoats tidal flat consists of three depositional environments that are arranged broadly parallel to shoreline, consisting of a mud flat (3.0 to 3.5 m elevation), mixed (sand and mud)-flat (0.6 to 3.0 m elevation), and sand flat (< 0.6 m elevation) (Figs. 1B, 2A). These three depositional environments represent an evolution from the saltmarsh-fringed landward margin of the tidal flat to the ebb channel.

The mud flat has a surface that is composed of fluidized mud, algal mats, bird tracks, and a pimpled surface (Fig. 2B, C). The sand flat contains extensive low amplitude (approximately < 1 m) 2D dunes (Fig. 2F) with surface bedforms dominated by straight-to-lingoid current ripples. The mixed tidal flat, has a distinct biotic zonation dominated by lugworms (*Arenicola marina*). Tube-like faecal mounds (Fig. 2D, E) overprint the gradational transition from an upper, structureless muddy surface to a lower current ripple dominated texture.

The whole tidal flat is drained by a network of dendritic tidal creeks. There is a morphological evolution from approximately 50 cm wide channels (Fig. 2I, J) in the mud flat, with lower channel axes composed of bioclasts and granule to pebble lag deposits, to m-wide, meandering, channelized systems that erode down to depths of ~ 2 m in the mixed flat, with a current rippled and bioturbated base (Fig. 2I).

The spatial distribution of surface sediment properties in terms of grain size, clay fraction, and sorting is presented in Figure 4 with values summarised in Table 1. There is a broad trend of decreasing grain size (from upper medium sand- to silt dominated-assemblages), increasing clay fraction content (from 0.3 to 10.5 %), and reduced sorting (from well sorted to very poorly sorted) towards the tidal limit (Fig. 4B-D). The surface sediment type is illustrated via SEM (texture) and SEM-EDS (mineralogy) images (Figs. 5, 6).

The clay-fraction is dominated by illite, with smaller, broadly equal, quantities of chlorite and kaolinite (Table 2). The clay mineral assemblage is distributed principally as clay coats on or between grains (approximately 80-90 %) (Fig. 6), as clay-rich rock fragments, or as clumps of clay material that potentially resulted from flocculation. In the sand flat samples, the clay-fraction component occurs

almost exclusively as discontinuous coats on sand-grain surfaces, with the greatest thickness occurring at grain indentations and embayments (Figs. 5, 6). In the tidal flat sediments, illite, chlorite, and kaolinite are all mainly present as grain-coats and bridging-structures. Chlorite is also associated with clay-rich lithic grains (Fig. 6). Illite and kaolinite also occur within, and on, feldspar grains (Fig. 6). The carbonate content of the sediments is highest in the mud flat samples (Table 2).

4.2. Near-surface depositional architecture and sediment characteristics

Detailed facies descriptions, used to cross-check the validity of the utilised sand-mud ratio classification scheme, are given in Table 3; sediment characteristics from the near-surface are presented in Table 1. Sedimentary logs summarising grain size, sedimentary structure, bioturbation index, clay fraction percentage, and clay-coat abundance are presented in Figure 3.

Both the landward decrease in surface sediment grain size and increase in clay fraction content (Fig. 4C) are broadly replicated in the sediment cores that range from medium sand to silt, hosting a 0.2 to 12 % clay fraction percentage. It is not possible to uniquely correlate beds between the five cores even though they occur within 500 m (Fig. 3). There is no systematic increase in the proportion of sediment clay fraction with depth (Fig. 3). Also, there is no systematic variation of clay-coat coverage with increasing depth for each individual sediment facies or each core (Table 4, Fig. 3).

4.3. Biological activity and indicators

Surface biological activity

Lugworm faecal cast density displays clear biogenic zonation across the tidal flat (Figs. 2D, E, 4E) with the greatest cast density found in the intermediate, mixed

tidal flat environments (> 50 faecal casts per m^2). Lugworms are largely absent in the mud flat as shown by the lack of faecal casts (compare Fig. 1B to 3E). Lugworms showed a decreasing abundance with proximity to the ebb channel in the sand flat (compare Fig. 1B to 3E).

Chlorophyll-a varies from 11.8 to 46.8 µg/g across the tidal flat (Fig. 4F). There is local heterogeneity of chlorophyll-a depicted in Figure 4F, but there is a trend of increasing abundance towards the tidal limit. There is a clear difference in biofilm abundance between depositional environments with an average 38.4 µg/g (n = 6) in mud flats, 17.7 µg/g (n = 7) in mixed flats, and 13.4 µg/g (n = 4) in sand flats (Table 1). This indicates that the greatest abundance of sediment-colonising, biofilm-producing diatoms (MPB) and such biofilm material occurs in the mud flat, with much less in mixed-tidal flats, and least in sand flat sediments (compare Fig. 1B to Fig. 4F).

Diatoms and biofilms are present in surface sediments as aggregates in association with clay-grade material, typically attached to sand-grain surfaces (Fig. 5H). Biofilms are present in dehydrated form (an artefact of sample preparation) as thin, wrinkled films coating sand-grain surfaces (Fig. 5G). A network of fine, fibrous filaments occur in surface sediments (Figs. 5, 6) to create linkages between sand grains; a textural characteristic previously shown to be derived from clay mineral attachment on a biofilm (EPS) root structure (Vos et al., 1988; Hoagland et al., 1993; De Winder et al., 1999; Higgins et al., 2003; Malarkey et al., 2015; Wooldridge et al., 2017a). As a result of sample preparation of near-surface sediment (i.e., thin section construction), diatoms and biofilm film coatings are not identifiable, although the biologically-mediated clay-coat textures (i.e., clay linkages between grains) are present (Wooldridge et al., 2017a) (Fig. 7).

Near-surface biological activity

Using the qualitative bioturbation intensity scale proposed by Taylor and Goldring (1993), results showed that bioturbation intensity in near-surface, tidal flat, sediment varied from 0 (absent) to 6 (complete obliteration of original texture) (Fig. 3). Extensive bioturbation occurs in the mixed- and mud-tidal flat environments while relatively reduced amounts of bioturbation occurred in the sand flats.

Total carbohydrate sampling commenced at 5 cm depth, which is well below the depth reported for typical, active diatom biofilm production (4 to 5 mm) (Hoagland et al., 1993; Stal, 2003). This strategy was implemented to avoid active (present day) biofilm growth masking patterns of palaeo-biofilm abundance (Fig. 4F). The data indicate that carbohydrate is pervasively present in tidal flat sediment but with a heterogeneous abundance distribution (Fig. 8). Sand flat sediments have an average carbohydrate content of 192.6 μg/g, mixed flats have 759.0 μg/g, and mud flats have 767.8 μg/g (Table 1). The pattern of increased sediment biofilm abundance in mud- and mixed- tidal flat environments is comparable to surface sediments (compare Fig. 4F to Fig. 8). The total carbohydrate fraction has a positive correlation with increasing clay fraction percentage, and a negative correlation with increasing mean sediment grain size (Table 4). There is no statistical correlation between total sediment carbohydrate and depth (Fig. 8, Table 4).

4.4. Characteristics of clay-coated sand grains: morphology and mineralogy

Clay coats cover all component grains (Fig. 6). Tidal flat clay coats consist of a network of partial grain coating and grain-linking, fibrous filaments composed of clay minerals and clay- to silt-sized material (organics, lithics, and clay minerals)

capable of coating up to 76 % of 2D grain surfaces. Clay coats are thickest in the mud- and mixed-tidal flat sediments (Fig. 6).

Clay coats in the sand flat samples (both surface and near-surface) occur as discontinuous thin coats, with greatest thickness in grain indentations; there is an absence of fibrous linkages between grains in sand flat sediments (Fig. 6). Figures 5 (surface) and 7 (near surface) reveal no obvious differences in the textural characteristics of surface and near-surface clay coats. No grain supporting clay matrix material was present in any of the imaged samples.

Clay coats are composed of illite, chlorite and kaolinite, each identified using both SEM-EDS and routine secondary X-ray analysis using the Hitachi TM3000 SEM (Figs. 6, 9, 10, Table 2). There was no difference in observed clay-coat mineralogy between clay coats on different framework grains (e.g., bioclasts, quartz, or feldspars) (Fig. 6). The mineralogy of clay coats, derived by SEM-EDS analyses, is comparable to the whole sediment, clay mineral assemblage (as determined by X-ray diffraction analysis) previously published for the Ravenglass estuary (Daneshvar, 2011; Daneshvar and Worden, 2017; Wooldridge et al., 2017b). Bulk clay mineralogy is here reported as index values (e.g., illite/(illite + chlorite + kaolinite)) (employing the assumption that the majority of the sediment's clay mineral content is present as clay coats) to constrain the relative distribution trends of the grain coating clay mineral assemblage. Figures 9 and 10 show that clay-coat mineralogy varies across tidal flat sediments.

The clay-coat mineralogy of both surface and near-surface sediment (Figs. 9,10, respectively) have a mineralogy composed of illite, chlorite and kaolinite with a minimum 60 % of the clay minerals composed of illite. The relative proportion of clay-coating chlorite is highest in the coarser-grained (higher energy) sand flat

samples. The surface trend of decreasing illite and increasing chlorite proportions with progression from the mud- to sand flat is replicated in near-surface sediment (e.g., compare Figs. 9 and 10). A key observation is that clay-coat mineralogy is not homogeneous across tidal flat sediments.

4.5. Clay-coat distribution

Clay-coat coverage surface variability

Clay coats are heterogeneously distributed across surface and near-surface tidal flat sediments (Figs. 3, 9). The degree of clay-coat coverage ranged from 3.4 to 69.4 % (Table 1). Clay-coat coverage increases towards the upper tidal limit, revealing a landward increase, with average clay-coat coverage of 3.9 % for sand flat, 28.7 % for mixed flat, and 61.7 % for mud flat sediment assemblages (Fig. 9). There is also heterogeneity in the proportion (percentage of measured grains) of grains devoid of clay coats; sand flats have 43 %, mixed flats have 6 %, and mud flats have 1 %, respectively.

Clay-coat coverage: near-surface variability

The heterogeneous distribution of clay-coat coverage in near-surface sediment is illustrated in Figures 3 and 10. Clay coats from intervals with a high sand percentage (> 90 %), and textural characteristics consistent with a sand flat environment of deposition (Fig. 3), have the lowest average percentage clay-coat coverage 15.7 % with 24 % of measured grains devoid of coats. Samples from mixed- and mud flat intervals have average grain coverage values of 42.8 % and 61.9 %, respectively. Clay-coat coverage increases in more heterolithic intervals and those typically characterised by increased bioturbation intensity (Fig. 3).

4.6. Correlations between clay-coat coverage, depth, sedimentological, and biological data sets

Figures 3, 10 and Tables 2, 4 show that, despite increased clay-coat coverage values for mixed- and sand flat intervals in near-surface sediment (compared to surface samples), there is no identifiable increase with depth. Pearson's correlation was used to test the statistical significance between clay-coat coverage and depth. This approach was first applied to the whole data set (Table 4) and subsequently undertaken on samples categorised via sand percentage (sand-mud ratio) into a consistent depositional environment framework (values stated below) (i.e., surface mixed flat compared to near-surface mixed flat samples). The first approach showed that there is no relationship between depth and clay coat coverage (Table 4). The second approach confirmed that there is no relationship between depth and clay-coat coverage even when sediment type is taken into account. Clay-coat coverage when compared to depth for samples categorised via sand percentage revealed a Pearson's correlation of -0.16 with a P value of 0.71, 0.05 with a P value of 0.81, and 0.28 with a P value of 0.31, for mud-, mixed-, and sand flat samples, respectively. The data thus show that there is no statistical link between overall clay-coat coverage and depth (illustrated in Fig. 3, 11D), and no statistically identifiable post depositional increase in clay-coat coverage with depth for each depositional environment (sediment facies).

Textural analysis has identified clear differences between tidal flat depositional environments, both in terms of sediment characteristics (Table 1, Figs. 2, 5, 6, 8) and biofilm abundance (Fig. 4F, 7, Table 1). A Pearson's correlation matrix was used to test the statistical significance of the entire surface and near surface data sets (Table 4). There is significant correlation between the extent of clay-coat coverage and sediment heterogeneity in the form of grain size, sorting and clay fraction percentage (Fig 11, Table 4).

Clay-coat coverage has been plotted as a function of sediment heterogeneity for surface and near-surface sediment (Fig. 11) with the percentage clay-coat coverage increasing in a linear trend with a decreasing grain size and increasing clay fraction percentage. Figure 11 shows that a very fine sand with > 7 % clay fraction is necessary for extensive clay-coat coverage (defined here as > 50 % average grain coverage); these conditions are found in mud- and mixed-tidal flat environments.

The surface distribution characteristic of the lugworm population does not spatially correlate to the degree of clay-coat coverage (compare Fig. 4E to Fig. 9), with mud flats devoid of an extensive lugworm population. The bioturbation intensity recorded in near-surface sediment (Fig. 3) showed no correlation to the extent of clay-coat coverage (Fig. 12).

Figure 13 and Table 4 show a strong, statistical correlation between the degree of clay-coat coverage and sediment biofilm abundance for both surface (chlorophyll-a content) and near-surface (total carbohydrate) sediment. Clay-coat coverage thus increases with an increased abundance of sediment biofilms (Figs. 10, 13, compare Fig. 4F to Fig. 9).

5. Discussion

5.1. Origin of the sedimentological and biological characteristics of the Saltcoats tidal flat

Tidal flats typically exhibit zonation in grain size, clay fraction percentage, and surface morphology (Amos, 1995), which has been reported to result from the dominant hydrological conditions (i.e., velocity asymmetry between flood and ebb currents) (Amos, 1995; Yang et al., 2005). The Saltcoats tidal flat sediments

(surface and near-surface) show a comparable landward decrease in sediment grain size and increased sediment heterogeneity.

The clay fraction occurs principally as clay coats in the sand-dominated sediment samples (mixed- and sand flat) of the Saltcoats tidal flat (Fig. 6), explaining the strong correlation between clay-fraction percentage and clay-coat coverage (Table 4 & Fig. 11B). It is likely that the mechanism that controls the occurrence of clay-coats also strongly influences heterogeneity in tidal-flat sediments. The correlation between clay fraction percentage and the environment of deposition across tidal flat sediments suggests that sediment heterogeneity is controlled by clay particle entrapment at the site of deposition.

The landward increase in sediment biofilm abundance in surface sediment (chlorophyll-a) indicates that mixed- and mud-tidal flat environments are extensively colonized by biofilm-producing diatoms. The distribution pattern for the Saltcoats tidal flat is comparable to that reported for the Severn Estuary, between England and Wales (Underwood and Paterson, 1993), in which significantly higher concentrations of chlorophyll-a occurred in sediments towards the tidal limit (landward direction). Similarly, the chlorophyll-a distribution patterns for the Saltcoats tidal flat are comparable to the Fraser River Estuary, British Columbia, Canada (Jiménez et al., 2015), and the bays in the Ebro delta complex, Spain, (Delgado, 1989). The consistent biological trends indicate a common nature and suggest that diatom and biofilm abundance is broadly predictable in modern estuarine and deltaic tidal flats.

The negative trend of increasing chlorophyll-a abundance with a decreasing grain size (compare Fig. 4F to B,Table 4) has also been reported in tidal flat sediments of the Humber Estuary, UK, the Marennes Estuary, France, and the Dollard Estuary,

Netherlands (Paterson et al., 2000; De Brouwer et al., 2003). The positive correlation between biofilm abundance and clay fraction is less well established in the literature (Table 4). Koppel et al. (2001) reported that diatoms grow best in high clay fraction rich sediments, so that once EPS is excreted by the diatoms, it has the effect of trapping more clay-silt sized particles, producing more environmentally advantageous conditions and a positive feedback.

The near-surface pattern of elevated sediment biofilm abundance in finer grained sediment, resulting from mud and mixed tidal flats and the lack of a systematic pattern with depth, suggests that biofilm abundance is directly inherited from surface processes and is preserved in the accumulated sediment. Furthermore water insoluble carbohydrate fractions are probably tightly bound to sand-grain surfaces as biofilm (De Winder et al., 1999) and could serve to bind clay and other minerals to grains (Fig. 8).

The heterogeneous distribution and range in the concentrations of total carbohydrate with depth are broadly consistent with other near-surface studies (10 mm depth) (De Winder et al., 1999) and (20 mm depth) (Taylor and Paterson, 1998). However, it must be noted that a study on the scale of the work presented here, on the Saltcoats tidal flat, has not previously been published.

5.2. Biological control on sediment heterogeneity

Tidal flat clay fraction, mean grain size, and grain sorting values have been previously illustrated to partly derive from the preferential entrapment of clay- and silt- sized particles by biofilms (Garwood et al., 2015; Jones, 2017). Tidal flats consist of non-cohesive, unconsolidated sand, physically cohesive muds, and sticky, cohesive biofilms (Jones, 2017). The influence of biofilms in tidal flat sediment has been illustrated by Faas et al. (1993) in the Bay of Fundy, Canada, in

which a structureless mud flat, that had the natural biofilm artificially removed by a biocide was transformed into a non-cohesive, rippled silt-flat in four tidal cycles (i.e., 2 days). Biofilms therefore are pivotal in controlling sedimentary structures.

The correlation between grain size (and clay fraction) and biofilm abundance at Saltcoats is consistent with a study of the Minas Basin, Bay of Fundy, Canada (Garwood et al., 2015). Biofilm production is restricted to the top few centimetres of the sediment (where light penetrates) so that active, biofilm-mediated entrapment of clay minerals as clay coats is restricted to the sediment surface. The implication is that near-surface trends in biofilm abundance and clay fraction percentage (principally present as clay coats) directly results from the surface abundance of biofilm-excreting diatoms.

5.3. Textural characteristics of clay-coated sand grains in a tidal flat sedimentary package

A key output of this work is that clay-coat morphology is heterogeneous across the Saltcoats tidal flat (Fig. 6). The morphology of the clay-coated sand grains in this study are comparable with those reported from the tidal flats of the Anllóns Estuary, northwest Spain, and the Leirárvogur Estuary, Iceland (Dowey, 2013; Dowey et al., 2017). The evolution in clay-coat morphology between mud- and sand flat sediments could derive from; (i) the increased hydraulic energy in the sand flat leading to reduced colonisation by benthic diatoms, and commensurately less biofilm creation to bind clays to grain surfaces (Delgado et al., 1991; Stal, 2003), or (ii) the partial abrasive removal of primary clay-coat projections and bridging structures on grain mobilisation (Wilson, 1992).

In establishing the likely origin of clay coats and their distribution patterns it is worth comparing our interpretations to previously reported mechanisms of clay

mineral attachment to sand-grain surfaces. Clay coats in intertidal sediments have been explained by the sedimentological processes of inheritance, mechanical infiltration of fine grained material (clay) into a sand-dominated matrix via percolating water followed by and drying-adhesion (Moraes and De Ros, 1992; Wilson, 1992; Dowey et al., 2017) and biologically via macro-and micro-organism produced biofilms (McIlroy et al., 2003; Needham et al., 2005; Worden et al., 2006; Wooldridge et al., 2017a).

The intricate bridging morphology of clay coats reported in this study (Figs. 5, 6, 7) are consistent with previously reported biologically-mediated, clay-coat textural components (Wooldridge et al., 2017a) and comparable to the textures of biofilm (EPS) coatings in sediment (Vos et al., 1988; Malarkey et al., 2015). . It has been noted that the observed biofilm-producing diatoms (Fig. 5H) are associated with clay-coated grains of the Mandovi Estuary, India (Kessarkar et al., 2010). Based on the published images, it is also evident that biofilm-producing diatoms are associated with clay-coated grains of the Anllóns Estuary, Spain (Dowey, 2013).

5.4. Controls on the distribution of clay-coated sand grains in near-surface sediment

Trends in clay-coat coverage in the three sedimentary environments (mud-, mixed-, and sand flat) are broadly reflected in the clay-coat coverage in near-surface sediment (Table 1). Mud flats have the highest clay-coat coverage (surface, 61.7 %; near-surface sediment, 61.9 %), while sand flats have the least coverage (surface, 3.9 %; near-surface sediment, 15.7 %).

It is noteworthy that the clay-coat coverage of surface sand flat samples increases, on average, by a factor of 4 in near-surface sediment (Table 1); whereas

clay-coat coverage of surface mixed flat samples increases on average by a factor of 1.5. Mud flats do not show any significant variation in clay-coat coverage.

Any sand flat package that is overlain by mud- or mixed-tidal flat sediments is unlikely to undergo infiltration at the present day, but it may have experienced infiltration when exposed at the surface. In addition, clay content may be incorporated into the sediment through bioturbation, from overlying clay-rich facies (Needham et al., 2005). At the surface, mud flats act as a largely impermeable barrier to pore-waters laden with clay, thus creating fluidised-mud (Fig. 2B). Consequently, any underlying 'clean sands' are unlikely to experience infiltration that would have led to any substantial, post-depositional increase in clay-coat coverage.

The lack of a systematic increase in clay-coat coverage with depth, or even in a bed (corresponding to a single sedimentary environment, Fig. 3) seems to suggest that m infiltration is not occurring at the present day. The absence of a statistically-significant, m-scale trend in the extent of clay-coat coverage between surface and near-surface sediment (Figs. 3, 11D), suggests that the possible post-depositional processes of infiltration and bioturbation have not significantly affected primary depositional (top few cm) trends in clay-coat characteristics.

The implication from Figure 3 is that the trend and distribution of clay-coated sand grains in near-surface sediment are principally controlled by surface-based processes. This observation is in accordance to the study by Buurman et al. (1998) in which they argued that due to the typical flocculation of clays and suspended clay- to silt-sized material, the upper pores of the sediment will become clogged and thus extensive infiltration-derived penetration of clay material into course sediment (e.g., sand flats) is unlikely.

Depositional environment thus exerts a dominant control on the characteristics of clay coats in tidal flat sediment (Table 4); this has been reasonably well established based on previous studies (Ehrenberg, 1993; Dowey, 2013; Wooldridge et al., 2017b). Cores from the Anllóns Estuary, Spain (Dowey et al., 2017) revealed a heterogeneous subsurface distribution of the extent of clay-coated sand grains as a function of the original environment of deposition. The similar trends in clay-coat coverage between the Saltcoats tidal flat and the tidal flats of the Anllóns Estuary, Spain (Dowey et al., 2017), suggest that this is a general feature of tidal flats.

The post-depositional process of infiltration has been proposed for arid to semi-arid environments due to fluctuating water tables (Matlack et al., 1989; Wilson, 1992). However, infiltration of sediment laden waters through the estuarine sediments at the Saltcoats tidal flat, Ravenglass Estuary, has no more than a secondary role in increasing clay-coat coverage and certainly does not alter primary (surface) clay-coat coverage patterns (Fig. 3, 9). This is most likely due to infiltration being inhibited by clay-rich beds (e.g., Fig. 3) which act as baffles.

Animal-sediment interaction-induced sediment mixing, particularly in the highly bioturbated intervals typical of mud and mixed tidal flats, may have contributed to elevated clay-coat grain coverage, but does not directly explain the distribution patterns of clay coats in the surface or near-surface (compare Figs. 4 to 9, 12).

The spatial distribution of surface clay fraction (XRD) mineralogy for Saltcoats was documented in Griffiths (2018) to display a relative increase of illite and decrease in chlorite towards the landward margin (i.e., mixed- and mud flats). This pattern is commensurate with clay-coat mineralogy of the surface and near-surface sediment, reported here (Figs. 9, 10). The relative enrichment of illite in the finer

sediment and chlorite in the coarser sediment was interpreted in Griffiths (2018) to result from hydraulically-controlled fractionation as a function of the grain size of different clay minerals in this estuary. Figure 6 shows that chlorite in clay coats typically occurs as larger "flakes" compared to illite.

The similarity of bulk clay-coat mineralogy (Fig. 9) and fine fraction mineralogy (XRD) previously reported for the estuary (Wooldridge et al., 2017b) suggests that the attachment mechanism does not preferentially adhere particular clay minerals and instead clay-coat mineralogy reflects the local clay mineral sediment assemblage. The result is that clay-coat mineralogy is principally controlled by: (i) provenance patterns and local physicochemical processes (e.g., weathering) that lead different phyllosilicates to have different grain sizes and (ii) by the estuarine hydrologically controlled segregation of the clay mineral assemblage (i.e., chlorite dropped out of suspension closer to the main ebb channel resulting in sand flats enriched in chlorite).

Surface clay-coat mineralogy is similar to clay-coat mineralogy in near-surface sediment, with chlorite most enriched in the sand flat sediments. However, the near-surface sand flat facies have a slightly higher chlorite index than the surface sediments as well as containing a slightly higher clay fraction (Tables 1, 2).There seems to be at least two possible explanations; (i) if local infiltration occurred when sand flat sediments were at the surface than it is likely that the infiltrating clay mineral assemblage was relatively enriched with chlorite, or (ii) the variation in chlorite content in near-surface sand flats, falls within the realm observed in surface sediment (i.e., sand flats which are more proximal to mixed-tidal flats are relatively clay fraction and chlorite enriched) (Wooldridge et al., 2017b).

If large-scale post-depositional infiltration of clay minerals had occurred through the near-surface sediments then a more regular signature (i.e., the fractionated depositional surface clay assemblage) may be expected. The surface and near-surface clay coats show trends of distribution and mineralogy identical to surface sediments and there is a marked lack of a regular distribution with depth. This strongly suggests that clay-coat mineralogy and distribution trends in near-surface sediment are principally controlled by the surface based attachment of the locally deposited clay mineral assemblage.

5.5. Implications for the origin and prediction of clay-coated sand grains in tidal flat sediments

The relationship of clay-coat coverage to grain size and the magnitude of the clay fraction is consistent with other reported surface based distribution models from the Anllóns Estuary, Spain, and Leirárvogur Estuary, Iceland (Dowey, 2013; Dowey et al., 2017). The formation of clay-coated sand grains in sedimentary environments can only occur in sediment that contains fine grained material (clay). Hence the correlation between clay coats and fine grain size, high clay fraction, and poorly sorted sediment can be expected since it is characteristic of low energy, tidal flat hydrological conditions (Flemming, 2012). In contrast, sediments deposited in high energy environments that lack means to accumulate clay cannot easily develop clay-coated sand grains. However, this study has provided a link between microbiological activity, the resulting bio-glue and clay mineral attachment to sand-grain surfaces (Wooldridge et al., 2017a). The abundance of sedimentary biofilms is controlled by the environmental niche of the biofilm excreting organisms (dominated by diatoms) which is primarily a function of hydrodynamic conditions in an estuary (Underwood and Paterson, 1993; Stal, 2003).

This study has shown that post-depositional bioturbation and infiltration seem to be less important than has been previously suggested. The implication is that distribution, grain coverage extent and mineralogy of clay-coated sand grains in near-surface sediments results from surface-controlled processes with a strong influence of the local sedimentary environment. Infiltration and bioturbation have a possible secondary role in increasing clay-coat coverage but do not alter the primary (surface) trends in clay-coat coverage or mineralogy patterns.

The generation of sedimentary and biological proxies for the extent of clay-coat coverage offers a crucial step towards building a credible capability for making predictions about grain coat coverage in ancient and deeply-buried reservoir rocks. The observation that the principal controls on the occurrence and extent of clay-coated sand grains in near-surface sediment are the biological and sedimentological conditions at the site of deposition is fundamental. If specific depositional environments can be predicted using seismic data, wireline logs, core, and cuttings then it may be possible to start predicting where, and to what extent, grain coating clays are present by applying surface based analogue models of clay-coat coverage (Dowey et al., 2017; Wooldridge et al., 2017b).

6. Conclusions

1. Tidal flat grain size varies from silt to medium sand, the clay fraction varies from 0.2 to 12.2 % and sorting varies from well sorted to very poorly sorted. The clay-fraction occurs principally as clay coats and bridging structures between sand grains. Biofilm abundance in surface sediments increases from the channel axis to the shore and thus increases from sand flats to mixed flats and then to mud flats.

2. Clay coats are characterised as discontinuous accumulations of illite, kaolinite, and chlorite clay minerals, silt- to clay-sized lithics, and bioclasts (e.g., diatoms) forming coating and bridging structures between sand grains.

3. Clay-coat coverage ranges from 2.5 to 76 %. In tidal flat sediments, an assemblage composed of a very fine sand that contains > 7 % clay-grade material is required to create extensive (> 50 %) clay coat grain coverage. These conditions are met in the mixed- and mud flat environments.

4. Clay-coat coverage is higher in near-surface sediment than the surface for the mud, mixed, and sand flat samples with a 0.2 %, 13 %, and 11.8 % increase, respectively. However, relative trends in clay-coat coverage are consistent between surface and near surface tidal flat sediment. Therefore the generation and distribution of clay-coated sand grains is principally controlled by surface-based processes local to the site of deposition.

5. The strong statistical correlation between clay coat coverage and biofilm abundance, the consistent biologically-mediated (biofilm) textures of clay-coated sand grains, and the absence of a pervasive post-depositional increase in the extent of clay-coat coverage, all suggest that clay coats are principally the result of biofilms derived from the normal life activities of diatoms. The post-depositional processes of infiltration and bioturbation have a possible secondary role in increasing clay-coat coverage but do not significantly alter primary depositional (surface) trends in clay-coat coverage.

Acknowledgements

The authors would like to thank the industrial members of the Chlorite Consortium who funded this research at Liverpool University: BP, BG (now Shell),

Statoil, Eni, Petrobras and Woodside. Especial thanks are offered to FEI (now ThermoFisher) for providing the QEMSCAN, with huge gratitude expressed to Prof Alan Butcher for facilitating this provision.

Reference list

Ajdukiewicz, J.M., Larese, R.E., 2012. How clay grain coats inhibit quartz cement and preserve porosity in deeply buried sandstones: Observations and experiments. American Association of Petroleum Geologists Bulletin 96, 2091-2119.

Amos, C.L., 1995. Siliciclastic tidal flats. Developments in Sedimentology 53, 273-306.

Armitage, P.J., Worden, R.H., Faulkner, D.R., Aplin, A.C., Butcher, A.R., Iliffe, J., 2010. Diagenetic and sedimentary controls on porosity in Lower Carboniferous fine-grained lithologies, Krechba field, Algeria: A petrological study of a caprock to a carbon capture site. Marine and Petroleum Geology 27, 1395-1410.

Billault, V., Beaufort, D., Baronnet, A., Lacharpagne, J.C., 2003. A nanopetrographic and textural study of grain-coating chlorites in sandstone reservoirs. Clay Minerals 38, 315-328.

Bloch, S., Lander, R.H., Bonnell, L., 2002. Anomalously high porosity and permeability in deeply buried sandstone reservoirs: Origin and predictability. American Association of Petroleum Geologists Bulletin 86, 301-328.

Brockamp, O., Clauer, N., 2012. Clay mineral provinces in tidal mud flats at Germany's North Sea coast with illite K-Ar ages potentially modified by biodegradation. Estuarine Coastal and Shelf Science 107, 32-45.

Brockamp, O., Zuther, M., 2004. Changes in clay mineral content of tidal flat sediments resulting from dike construction along the Lower Saxony coast of the North Sea, Germany. Sedimentology 51, 591-600.

Buurman, P., Jongmans, A., PiPujol, M., 1998. Clay illuviation and mechanical clay infiltration—Is there a difference? Quaternary International 51, 66-69.

Chakrabarti, A., 2005. Sedimentary structures of tidal flats: a journey from coast to inner estuarine region of eastern India. Journal of Earth System Science 114, 353-368.

Chang, J., Choi, J., 2001. Tidal-flat sequence controlled by Holocene sea-level rise in Gomso Bay, west coast of Korea. Estuarine, Coastal and Shelf Science 52, 391-399.

Daneshvar, E., 2011. Role of provenance on clay minerals and their distribution in modern estuaries . Ph.D. Thesis, Liverpool Univ. Liverpool, UK.

Daneshvar, E., Worden, R.H., 2017. Feldspar alteration and Fe minerals In: Reservoir quality prediction in sandstones and carbonates. (eds: Armitage, P.J., Butcher, A., Churchill, J., Csoma, A., Hollis, C., Lander, R.H., Omma, J., Worden, R.H.), Geological Society Special Publication, 435, pp. 1-32.

De Brouwer, J., De Deckere, E., Stal, L., 2003. Distribution of extracellular carbohydrates in three intertidal mudflats in Western Europe. Estuarine, Coastal and Shelf Science 56, 313-324.

De Winder, B., Staats, N., Stal, L., Paterson, D., 1999. Carbohydrate secretion by phototrophic communities in tidal sediments. Journal of Sea Research 42, 131-146.

Delgado, M., 1989. Abundance and distribution of microphytobenthos in the bays of Ebro Delta (Spain). Estuarine, Coastal and Shelf Science 29, 183-194.

Delgado, M., De Jonge, V., Peletier, H., 1991. Effect of sand movement on the growth of benthic diatoms. Journal of Experimental Marine Biology and Ecology 145, 221-231.

Dowey, P.J., 2013. Prediction of clay minerals and grain coatings in sandstone reservoirs utilising ancient examples and modern analogue studies. Ph.D. Thesis, Liverpool Univ. Liverpool, UK.

Dowey, P.J., Hodgson, D.M., Worden, R.H., 2012. Pre-requisites, processes, and prediction of chlorite grain coatings in petroleum reservoirs: A review of subsurface examples. Marine and Petroleum Geology 32, 63-75.

Dowey, P.J., Worden, R.H., Utley, J., Hodgson, D.M., 2017. Sedimentary controls on modern sand grain coat formation. Sedimentary Geology 353, 46-63.

Ehrenberg, S.N., 1993. Preservation of anomalously high-porosity in deeply buried sandstones by grain coating chlorite - examples from the Norwegian continental shelf. American Association of Petroleum Geologists Bulletin 77, 1260-1286.

Faas, R.W., Christian, H.A., Daborn, G.R., Brylinsky, M., 1993. Biological control of mass properties of surficial sediments: an example from Starr's Point tidal flat, Minas Basin, Bay of Fundy. Nearshore and estuarine cohesive sediment transport, 360-377.

Flemming, B.W., 2012. Siliciclastic back-barrier tidal flats, Principles of Tidal Sedimentology. Springer, 231-267.

Folk, R.L., Ward, W.C., 1957. Brazos river bar. A study in the significance of grain size parameters. Journal of Sedimentary Petrology 27, 3-26.

Garwood, J.C., Hill, P.S., MacIntyre, H.L., Law, B.A., 2015. Grain sizes retained by diatom biofilms during erosion on tidal flats linked to bed sediment texture. Continental Shelf Research 104, 37-44.

Gier, S., Worden, R.H., Johns, W.D., Kurzweil, H., 2008. Diagenesis and reservoir quality of Miocene sandstones in the Vienna Basin, Austria. Marine and Petroleum Geology 25, 681-695.

Glasmann, J., Lundegard, P.D., Clark, R., Penny, B., Collins, I., 1989. Geochemical evidence for the history of diagenesis and fluid migration: Brent sandstone, Heather Field, North Sea. Clay Minerals 24, 255-284.

Griffiths, J., 2018. Compositional and textural variation in modern estuarine sands: Implications for sandstone reservoir quality. Ph.D. Thesis, Liverpool Univ. Liverpool, UK.

Higgins, M.J., Molino, P., Mulvaney, P., Wetherbee, R., 2003. The structure and nanomechanical properties of the adhesive mucilage that mediates diatom-substratum adhesion and motility. Journal of Phycology 39, 1181-1193.

Higgs, R., Shanmugam, G., Poffenberger, M., 2002. Tide-dominated estuarine facies in the Hollin and Napo (T and U) formations (Cretaceous), Sacha field, Oriente Basin, Ecuador: Discussion. AAPG Bulletin 86, 329-334.

Hoagland, K.D., Rosowski, J.R., Gretz, M.R., Roemer, S.C., 1993. Diatom extracellular polymeric substances: function, fine structure, chemistry, and physiology. Journal of Phycology 29, 537-566.

Jesus, B., Brotas, V., Ribeiro, L., Mendes, C., Cartaxana, P., Paterson, D., 2009. Adaptations of microphytobenthos assemblages to sediment type and tidal position. Continental Shelf Research 29, 1624-1634.

Jiménez, A., Elner, R.W., Favaro, C., Rickards, K., Ydenberg, R.C., 2015. Intertidal biofilm distribution underpins differential tide-following behavior of two sandpiper species (Calidris mauri and Calidris alpina) during northward migration. Estuarine, Coastal and Shelf Science, 155, 8-16.

Jones, S., 2017. Goo, glue, and grain binding: Importance of biofilms for diagenesis in sandstones. Geology 45, 959-960.

Kessarkar, P.M., Purnachandra Rao, V., Shynu, R., Mehra, P., Viegas, B.E., 2010. The nature and distribution of particulate matter in the Mandovi estuary, central west coast of India. Estuaries and Coasts 33, 30-44.

Koppel, J., Herman, P.M., Thoolen, P., Heip, C.H., 2001. Do alternate stable states occur in natural ecosystems? Evidence from a tidal flat. Ecology 82,3449-3461.

Lander, R.H., Larese, R.E., Bonnell, L.M., 2008. Toward more accurate quartz cement models: The importance of euhedral versus noneuhedral growth rates. American Association of Petroleum Geologists Bulletin 92,1537-1563.

Lloyd, J.M., Zong, Y., Fish, P., Innes, J.B., 2013. Holocene and Lateglacial relative sea-level change in north-west England: implications for glacial isostatic adjustment models. Journal of Quaternary Science 28, 59-70.

Malarkey, J., Baas, J.H., Hope, J.A., Aspden, R.J., Parsons, D.R., Peakall, J., Paterson, D.M., Schindler, R.J., Ye, L., Lichtman, I.D., 2015. The pervasive role of biological cohesion in bedform development. Nature communications, 6(6257).

Martinius, A.W., Ringrose, P.S., Brostrom, C., Elfenbein, C., Naess, A., Ringas, J.E., 2005. Reservoir challenges of heterolithic tidal sandstone reservoirs in the Halten Terrace, mid-Norway. Petroleum Geoscience 11, 3-16.

Matlack, K.S., Houseknecht, D.W., Applin, K.R., 1989. Emplacement of clay into sand by infiltration. Journal of Sedimentary Petrology 59, 77-87.

McIlroy, D., Worden, R.H., Needham, S.J., 2003. Faeces, clay minerals and reservoir potential. Journal of the Geological Society 160, 489-493.

Moraes, M.A.S., De Ros, L.F., 1992. Depositional, infiltrated and authigenic clays in fluvial sandstones of the Jurassic Sergie Formation, Reconcavo Basin, northeastrn Brazil. Origin, Diagenesis and Petrophysics of Clay Minerals in Sandstones. SEPM Special Publication 47, 197-208.

Needham, S.J., Worden, R.H., McIlroy, D., 2005. Experimental production of clay rims by macrobiotic sediment ingestion and excretion processes. Journal of Sedimentary Research 75, 1028-1037.

Paterson, D., Tolhurst, T., Kelly, J., Honeywill, C., De Deckere, E., Huet, V., Shayler, S., Black, K., De Brouwer, J., Davidson, I., 2000. Variations in sediment properties, Skeffling mudflat, Humber Estuary, UK. Continental Shelf Research 20 1373-1396.

Saïag, J., Brigaud, B., Portier, É., Desaubliaux, G., Bucherie, A., Miska, S., Pagel, M., 2016. Sedimentological control on the diagenesis and reservoir quality of tidal sandstones of the Upper Cape Hay Formation (Permian, Bonaparte Basin, Australia). Marine and Petroleum Geology 77, 597-624.

Schindler, R.J., Parsons, D.R., Ye, L., Hope, J.A., Baas, J.H., Peakall, J., Manning, A.J., Aspden, R.J., Malarkey, J., Simmons, S., 2015. Sticky stuff: Redefining bedform prediction in modern and ancient environments. Geology 43, 399-402.

Semeniuk, V., 2005. Tidal Flats. In: M.L. Schwartz (Ed.), Encyclopedia of Coastal Science. Springer , Dordrecht, pp. 965-975.

Stal, L.J., 2010. Microphytobenthos as a biogeomorphological force in intertidal sediment stabilization. Ecological Engineering 36, 236-245.

Stal, L.J., 2003. Microphytobenthos, their extracellular polymeric substances, and the morphogenesis of intertidal sediments. Geomicrobiology Journal 20, 463-478.

Stevens, V., 1991. The Beatrice Field, Block 11/30a, UK North Sea. Geological Society, London, Memoirs 14, 245-252.

Taylor, A., Goldring, R., 1993. Description and analysis of bioturbation and ichnofabric. Journal of the Geological Society 150, 141-148.

Taylor, I., Paterson, D., 1998. Microspatial variation in carbohydrate concentrations with depth in the upper millimetres of intertidal cohesive sediments. Estuarine, Coastal and Shelf Science 46, 359-370.

Underwood, G., Paterson, D., Parkes, R.J., 1995. The measurement of microbial carbohydrate exopolymers from intertidal sediments. Limnology and Oceanography 40, 1243-1253.

Underwood, G.J., Paterson, D.M., 1993. Seasonal changes in diatom biomass, sediment stability and biogenibilization in the Severn Estuary. Journal of the Marine Biological Association of the United Kingdom 73, 871-887.

Vos, P., De Boer, P., Misdorp, R., 1988. Sediment stabilization by benthic diatoms in intertidal sandy shoals; qualitative and quantitative observations, Tide-influenced sedimentary environments and facies. Springer, 511-526.

Wilson, M.D., 1992. Inherited grain-rimming clays in sandstones from eolian and shelf environments: their origin and control on reservoir properties. Origin, Diagenesis and Petrophysics of Clay Minerals in Sandstones. SEPM Special Publication 47, 209-225.

Wooldridge, L.J., Worden, R.H., Griffiths, J., Thompson, A., Chung, P., 2017a. Biofilm origin of clay-coated sand grains. Geology 45, 875-878.

Wooldridge, L.J., Worden, R.H., Griffiths, J., Utley, J.E., 2017b. Clay-coated sand grains in petroleum reservoirs: understanding their distribution via a modern analogue. Journal of Sedimentary Research 87, 338-352.

Worden , R.H., Armitage, P.J., Butcher, A., Churchill, J., Csoma, A., Hollis, C., Lander, R.H., Omma, J. (2018) Petroleum reservoir quality prediction: overview and contrasting approaches from sandstone and carbonate communities In: Reservoir quality prediction in sandstones and carbonates. (eds: Armitage, P.J., Butcher, A., Churchill, J., Csoma, A., Hollis, C., Lander, R.H., Omma, J., Worden, R.H.), Geological Society Special Publication, 435, pp. 1-32.

Worden, R.H., Burley, S.D., 2F003. Sandstone diagenesis: the evolution from sand to stone. Sandstone Diagenesis, Recent and Ancient. International Association of Sedimentologists Reprint Series, 3-44.

Worden, R.H., Morad, S., 2003. Clay minerals in sandstones: Controls on formation, distribution and evolution. Clay Mineral Cements in Ssandstones. International Association of Sedimentologists Special Publications 34, 3-41.

Worden, R.H., Morad, S., 2000. Quartz cementation in sandstones: a review of the key controversies. Quartz Cementation in Sandstones. International Association of Sedimentologists Special Publications, 1-20.

Worden, R.H., Needham, S.J., Cuadros, J., 2006. The worm gut; a natural clay mineral factory and a possible cause of diagenetic grain coats in sandstones. Journal of Geochemical Exploration 89, 428-431.

Yang, B., Dalrymple, R., Chun, S., 2005. Sedimentation on a wave-dominated, open-coast tidal flat, south-western Korea: summer tidal flat–winter shoreface. Sedimentology 52, 235-252.

Figure captions

Figure 1. Location and depositional environment maps of the Saltcoats tidal flat. (A) Location of Saltcoats in relation to the Ravenglass Estuary and the UK. (B) Map showing the study area and component depositional environments subdivided by sand percentage; mud flat (15-50 % sand), mixed flat (50-90 % sand), and sand flat (> 90 % sand) as defined by laser particle size analysis. (C) Aerial image of the Saltcoats tidal flat showing sample locations.

Figure 2. Photographs of geomorphic and sedimentary features of the Saltcoats tidal flat. (A) Overview of the study area; arrows mark the boundary between tidal flat environments. (B, C) Mud flat. (D, E) Mixed flat. (F, G) Sand flat. (H) Aerial image of the study area. Arrows indicate the location and direction of the photographs (A- J). (I) Channelized tidal creek network dissecting the lower mixed tidal flat. Note the rippled and bioturbated channel axis. (J) Tidal creek channel draining the mud flat and upper mixed tidal flat.

Figure 3. Sedimentological, clay-coat coverage, and clay fraction percentage logs of core from the Saltcoats tidal flat. Graphic logs of bioturbation intensity, clay-coat overage, and clay fraction illustrate the near-surface distribution characteristics. See (F) for an explanation of the symbols and location of cores.

Figure 4. Distribution maps of surface sedimentary and biological characteristics. (A) Map of tidal flat elevation. (B) Map of surface-sediment grain size. (C) Surface distribution of sediment clay fraction percentage. (D) Map of surface-

sediment sorting. (E) Map of lugworm population (faecal mound density). (F) Surface distribution of sediment biofilm abundance (chlorophyll-a).

Figure 5. Scanning electron microscopy (SEM) images of surface clay-coated sand grains. Arrows indicate regions and key textural characteristics of clay coats. SEM images of clay coats from mud flat (A, B), and mixed flat (C- F) sediments. SEM images of loose sediment grain stubs (G and H). The representative images illustrate (i) the intricate textural characteristics of clay coats (A- F), (ii) dehydrated biofilm coats on sand grains surfaces (white dashed line) (G), and (iii) the presence of biofilm excreting diatoms in clay-coat (red lines) (H).

Figure 6. Scanning electron microscope energy dispersive spectrometry (SEM-EDS) images of clay-coat mineralogy: mud flat (A- C), mixed flat (D- F), and sand flat (G-I) depositional environments. Arrows indicate regions and key textural characteristics of clay coats.

Figure 7. Scanning electron microscopy (SEM) images of near-surface clay-coated sand grains: mud flat (A, B), mixed flat (C, D), and sand flat (E, F) intervals. The position of the imaged sediment is illustrated in Figure 6 and correlated by the coloured circles 1, 2, and 3. Arrows indicate regions and key textural characteristics of clay coats.

Figure 8. Sedimentary log illustrating biofilm abundance in near-surface tidal-flat sediment: the appearance of dried core material (A), bioturbation intensity (Taylor and Goldring, 1993) (B), the environment of deposition (C), sedimentary characteristics (D), the near-surface variability in total carbohydrate content (E),

and scanning electron microscopy (SEM) images of the analysed intervals (F-H). For an explanation of the symbols and location of the core, see Figure 6F.

Figure 9. Map of surface sediment clay-coat coverage. (A) Areas in light purple signify minimal (< 10 %) partial clay-coat grain coverage, with dark purple to blue regions indicating extensive surface clay-coated sand grains. Pie charts indicate index values of clay-coat mineralogy. (B) Pie charts illustrating the average clay-coat mineralogy of depositional environments.

Figure 10. Synthesis log of correlated near-surface data sets. Bioturbation intensity (A), the environment of deposition (B), sedimentary log (C), total sediment carbohydrate (D), clay-coat coverage (E), clay fraction percentage (F), and clay-coat mineralogy (G). For an explanation of the symbols and location of the core, see Figure 6F.

Figure 11. Plot of mean grain size (A), sediment clay-fraction percentage (B), sorting (C), and sample depth (D) against clay-coat coverage.

Figure 12. Plot of near-surface bioturbation intensity against clay-coat coverage.

Figure 13. Plot of surface (chlorophyll-a) and near-surface (total carbohydrate) sediment biofilm abundance against clay-coat coverage.

Table 1. Sediment, biological, and clay-coat heterogeneity of the Saltcoats tidal flat

			Clay-coat coverage (%)	Mean grain size (µm)	Grain size sorting	Clay-fraction (%)	Chl-a (µg/g)	Total carbohydrate
surface	mud-flat	average	61.7	37.1	3.7	8.6	38.4	_
		max	69.4	43.7	4.2	10.5	46.8	_
		min	57.1	27.9	3.2	7.6	25	_
	mixed-flat	average	28.7	102.7	2.8	3.3	17.7	_
		max	43	159.7	4.3	7.2	27.5	_
		min	13	47.2	1.9	0.5	10	_
	sand-flat	average	3.9	213.3	1.5	1.2	13.4	_
		max	4.3	337.8	1.6	2	14.7	_
		min	3.4	143.7	1.3	0.3	11.8	_
near-surface sediment	mud-flat	average	61.9	37.8	4.1	10	_	767.8
		max	76	45.6	5.1	12.2	_	956
		min	50	30.1	3.3	6	_	579.6
	mixed-flat	average	42.8	104.3	3.1	5.8	_	759
		max	74.6	276.3	4.6	12.3	_	957.5
		min	13.4	48.3	1.9	2.3	_	461.9
	sand-flat	average	15.7	187.6	1.6	1.7	_	192.6
		max	24.2	311.4	1.8	3.4	_	256.6
		min	2.5	136.8	1.4	0.2	_	128.5

Table 2. Scanning electron microscope-energy dispersive spectrometry derived mineralogy of the Saltcoats tidal flat (values present as image area percentages).

		surface			Near-surface sediment		
		mud	mixed	sand	mud	mixed	sand
Clay index	Illite	0.8	0.78	0.75	0.73	0.67	0.62
	Kaolinite	0.08	0.09	0.06	0.08	0.14	0.05
	Chlorite	0.12	0.14	0.19	0.19	0.19	0.33
Quartz	_	65.55	75	82.18	69.81	69.18	82.52
Feldspars	_	13.26	11.49	9.47	14.53	14.02	9.96
carbonates	Calcite	2.74	2.51	1.14	4.67	3.28	1.63
	Dolomite	1.9	1.16	0.6	1.86	1.52	0.8
Mica	Muscovite	1.15	0.67	0.61	1.36	1.25	0.9
	Biotite	1.02	0.77	0.4	0.82	1.06	0.68

Table 3. Characteristic features and interpretations of core encountered near-

Dominant textures and sedimentary structures for each tidal-flat environments		Depositional processes and environment		Diagnostic textures and sedimentary structures of tidal-flat facies	Core geometry
Mud-flat (15-50 % sand): Sedimentary signature is characterised as intensely bioturbated to mottled texture, with a sparse to poorly preserved, silt dominated, and parallel laminated assemblage hosting	**Mud-flat (TF. 1.2.3)**	Mud-flat	Formed via the principal suspension settling of fine grained predominantly mud to silt size sediment during slack water with post-depositional intensive bioturbation.	**(TF.1)** Mottled (intensely bioturbated) clay- to silt-sized sediment.	Undulating upper contacts depicted predomina ntly by colour and grain size.

surface lithofacies of the Saltcoats tidal flat. The distribution of lithofacies is shown in Figure 3.

granule sized mud interclast, lithics, and minor fragmented bioclasts. **Mixed-tidal flat (50-90 % sand): Intervals consist of heavily bioturbated, parallel and ripple laminated silt-lower medium sand sized sediment. The laminated intervals present a decrease in thickness and abundance of sand layers with distance landward, cumulating in a heavily bioturbated to mottled texture. Ripple cross lamination is confined to coarse and clean sand intervals (i.e. > 78 % sand) representing the lower geographic extent of mixed-tidal-flats (Fig. 3.).** **Sand-flat (> 90 % sand): Intervals are characterised as alternating massive to ripple cross laminated, bioturbated fine to upper medium sand, hosting granule sized mud clasts, and pebble sized lithics.**		Mud-mixed flat	Alternating laminations of sand and silt represent tidal bundle/ couplets deposition, where each sand- to mud-lamination is produced by variations in tidal-current speed or by waves over a single tidal cycle (Martinius and Van den Berg, 2011). The difference between sand and silt layers derive from varying energy conditions during deposition. Laminations presents as horizontal, wavy, or discontinuous depending on the relative intensity of bioturbation.	**(TF.2)** Parallel laminated sand and silts	Commonly gradational contacts (owing to bioturbation intensity)
	Mixed-flat (TF 1.2.3. 4)	Mud-mixed flat	The relative abundance of sand vs silt is dependent upon original surface geographic position (see Figs. 2, and, with variable intensities of bioturbation up to sediment homogenization. These two facies thus form a continuum governed by the pro-gradation and retro-gradation of the tidal-flats determined by the landward extent of sand deposition and ripple formation. Ripple mud drapes deposit during periods of slack-water.	**(TF.3)** Bioturbated, laminated silt- to very fine-grained sand. Silt dominated, often intensely bioturbated (progressing to mottled texture in places) consisting of subordinate sand laminations and ripple laminations, hosting minor bioclastic debris and organics (rootlets).	Contacts are typically bioturbated or gradational
		Mud-mixed –sand flat		**(TF.4)** Bioturbated, rippled-laminated (sand-dominated), v.fine- to fine-sand. Sand-dominated, often intensely bioturbated (approaching mottled), with minor silt laminations, mud drapes (flaser bedding), and current ripples	Contacts are typically bioturbated or sharp-undulating
	Sand-flat (TF 4.5.)	Sand-flat	Low-amplitude tidal-dunes and ripple migration, proximal to the ebb-channel. The observed sparse mud drapes would have been deposited during low-tide.	**(TF.5)** Very fine- to medium-grained, cross-bedded and current-rippled sand. Mud-drapes and mud-intraclasts are rare.	Common erosive-undulating lower contact.
		Tidal creek	Represent lag deposits observed in the base of tidal creek channels (Fig. 2).	**(TF.6)** Lithic and bioclastic rich sand. Massive upper fine sand grade sediment hosting lithic and disarticulate bioclastic debris.	Sharp grain size defined contacts.

Table 4. Pearson's Correlation Coefficient matrix calculated from tidal flat sedimentological and biological data (Table 1). For P=-values < 0.05 (*), the correlation is statistically significant. P values of (P < 0.01) (**) and (p< 0.001) (***) represent very and extremely significant correlations, respectively.

	Clay-coat coverage (%)	Mean grain size (µm)	Grain size sorting (σg)	Clay-fraction (%)	Sand abundance (%)	Chl-a (µg/g)	Total carbohydrate (µg/g)	Depth (cm)
Clay-coat coverage (%)	x	0.000***	0.000***	0.000***	0.000***	0.002*	0.006*	0.134
Mean grain size (µm)	-0.75	x	0.000***	0.000***	0.000***	0.002*	0.003*	0.175
Grain size sorting (σg)	0.84	-0.76	x	0.000***	0.000***	0.005*	0.001*	0.542
Clay-fraction (%)	0.87	-0.7	0.76	x	0.000***	0.000***	0.013**	0.215
Sand (%)	-0.86	0.83	-0.87	-0.85	x	0.000***	0.011**	0.425
Chl-a (µg/g)	0.9	-0.7	0.65	0.95	-0.83	x	N/A	N/A
Total carbohydrate (µg/g)	0.86	-0.89	0.93	0.82	-0.83	N/A	x	0.069
Depth (cm)	-0.23	0.21	-0.09	-0.19	0.12	N/A	0.67	x

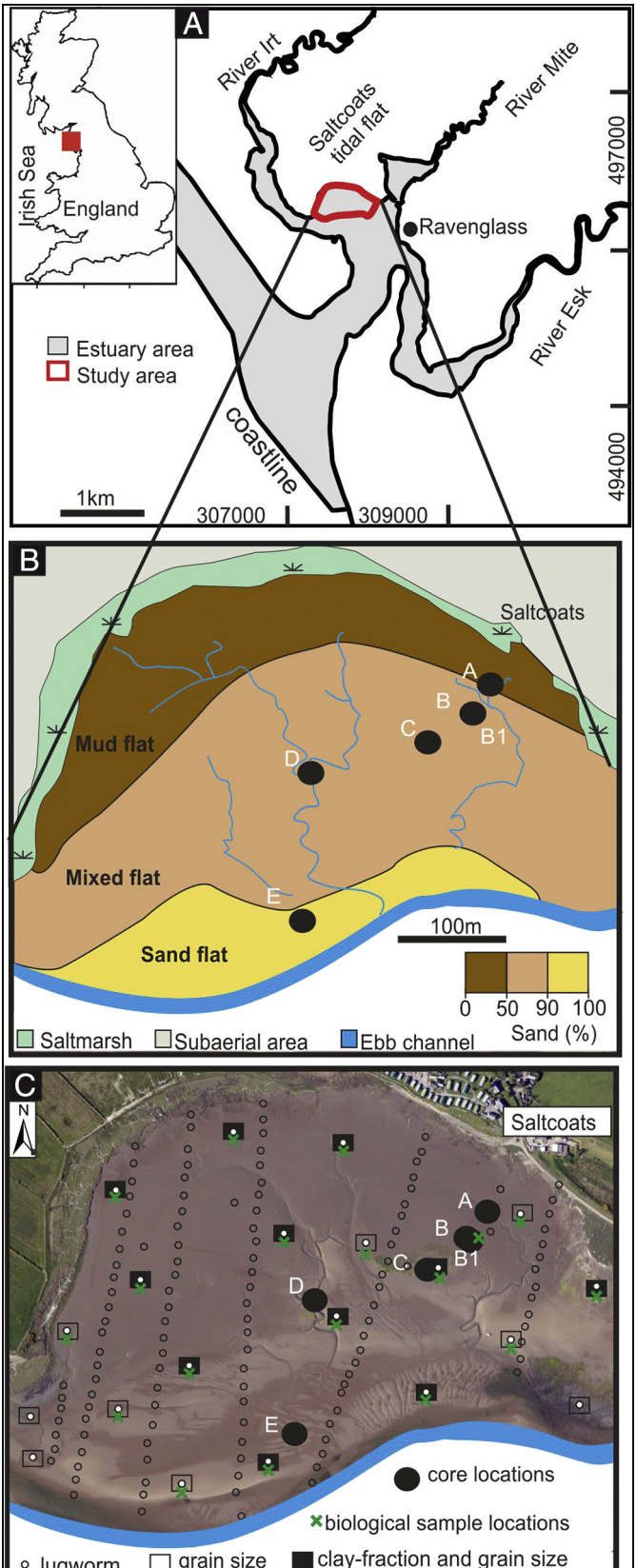
A
Irish Sea
England
River Irt
Saltcoats tidal flat
River Mite
Ravenglass
River Esk
497000
494000
Estuary area
Study area
coastline
1km
307000
309000
B
Saltcoats
A
B
C
B1
D
Mud flat
Mixed flat
E
Sand flat
100m
0 50 90 100
Sand (%)
Saltmarsh
Subaerial area
Ebb channel
C
N
Saltcoats
A
B
C
B1
D
E
core locations
biological sample locations
lugworm
grain size
clay-fraction and grain size

Figure 1

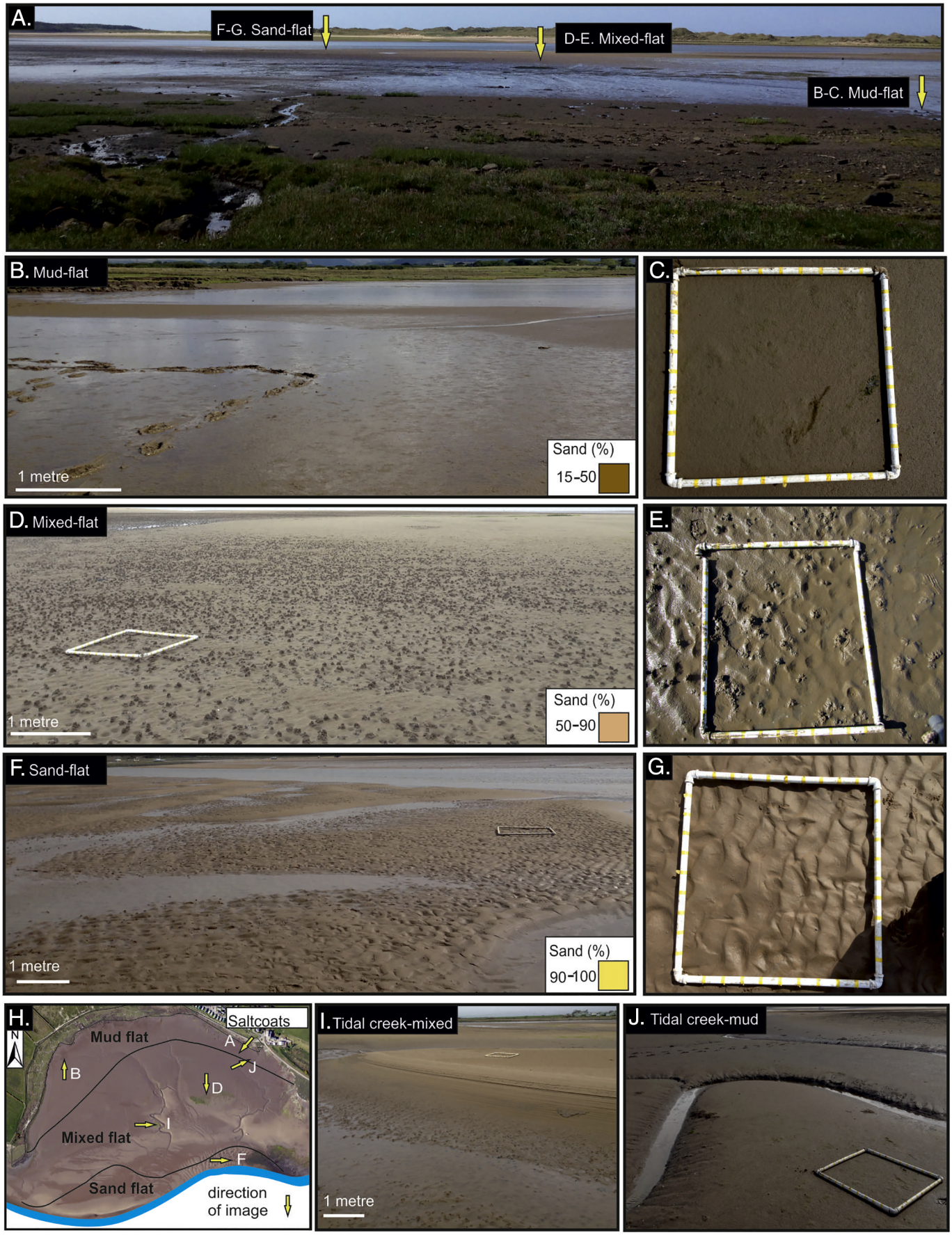
A.
F-G. Sand-flat
D-E. Mixed-flat
B-C. Mud-flat
B. Mud-flat
1 metre
Sand (%)
15–50
C.
D. Mixed-flat
1 metre
Sand (%)
50–90
E.
F. Sand-flat
1 metre
Sand (%)
90–100
G.
H.
Saltcoats
Mud flat
Mixed flat
Sand flat
direction of image
A
B
D
F
I
J
I. Tidal creek-mixed
1 metre
J. Tidal creek-mud

Figure 2

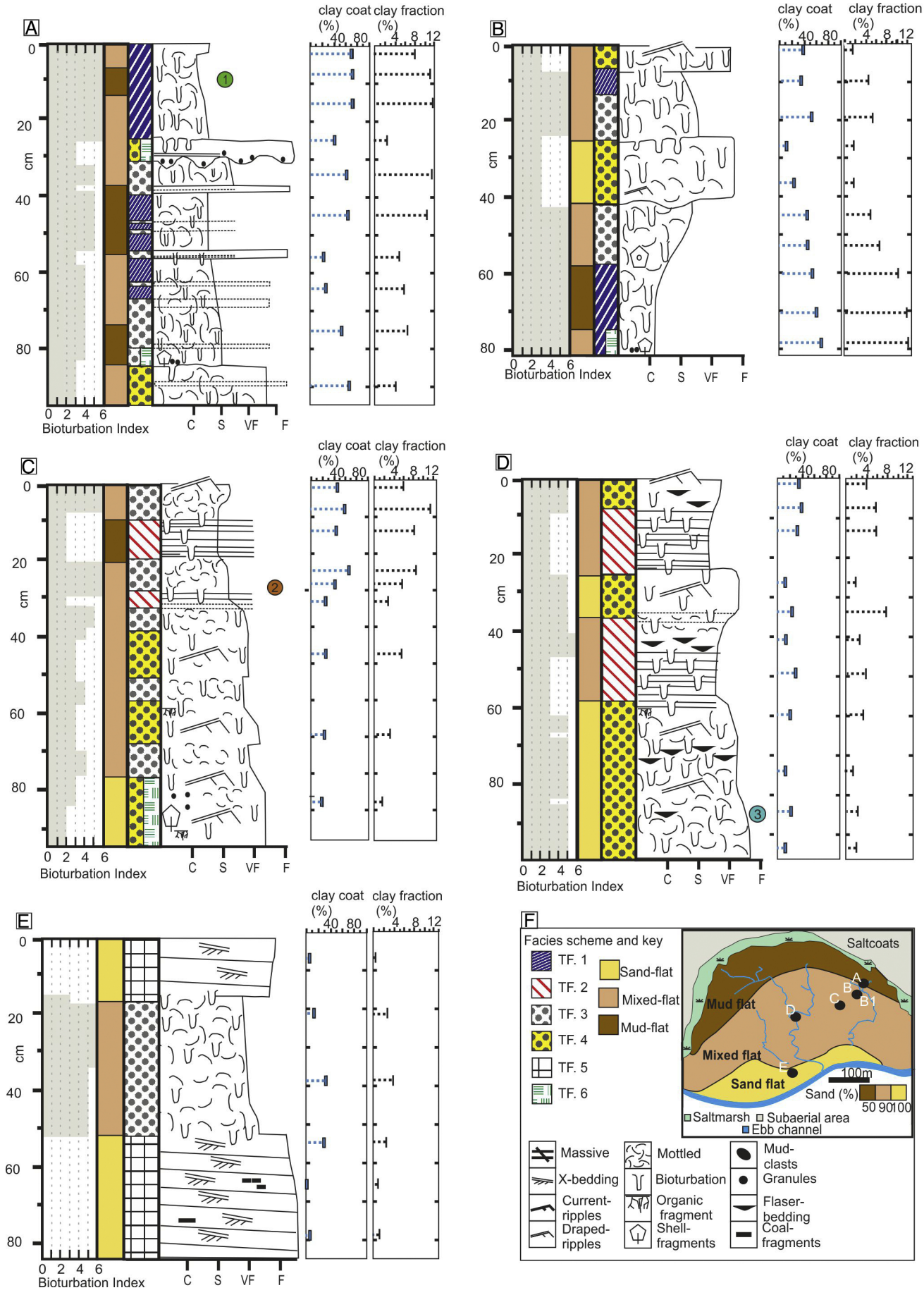
A
B
C
D
E
F
clay coat (%)
clay fraction (%)
40 80
4 8 12
cm
0 2 4 6
Bioturbation Index
C S VF F
Facies scheme and key
TF. 1
TF. 2
TF. 3
TF. 4
TF. 5
TF. 6
Sand-flat
Mixed-flat
Mud-flat
Saltcoats
Mud flat
Mixed flat
Sand flat
100m
Sand (%)
50 90100
Saltmarsh
Subaerial area
Ebb channel
Massive
X-bedding
Current-ripples
Draped-ripples
Mottled
Bioturbation
Organic fragment
Shell-fragments
Mud-clasts
Granules
Flaser-bedding
Coal-fragments

Figure 3

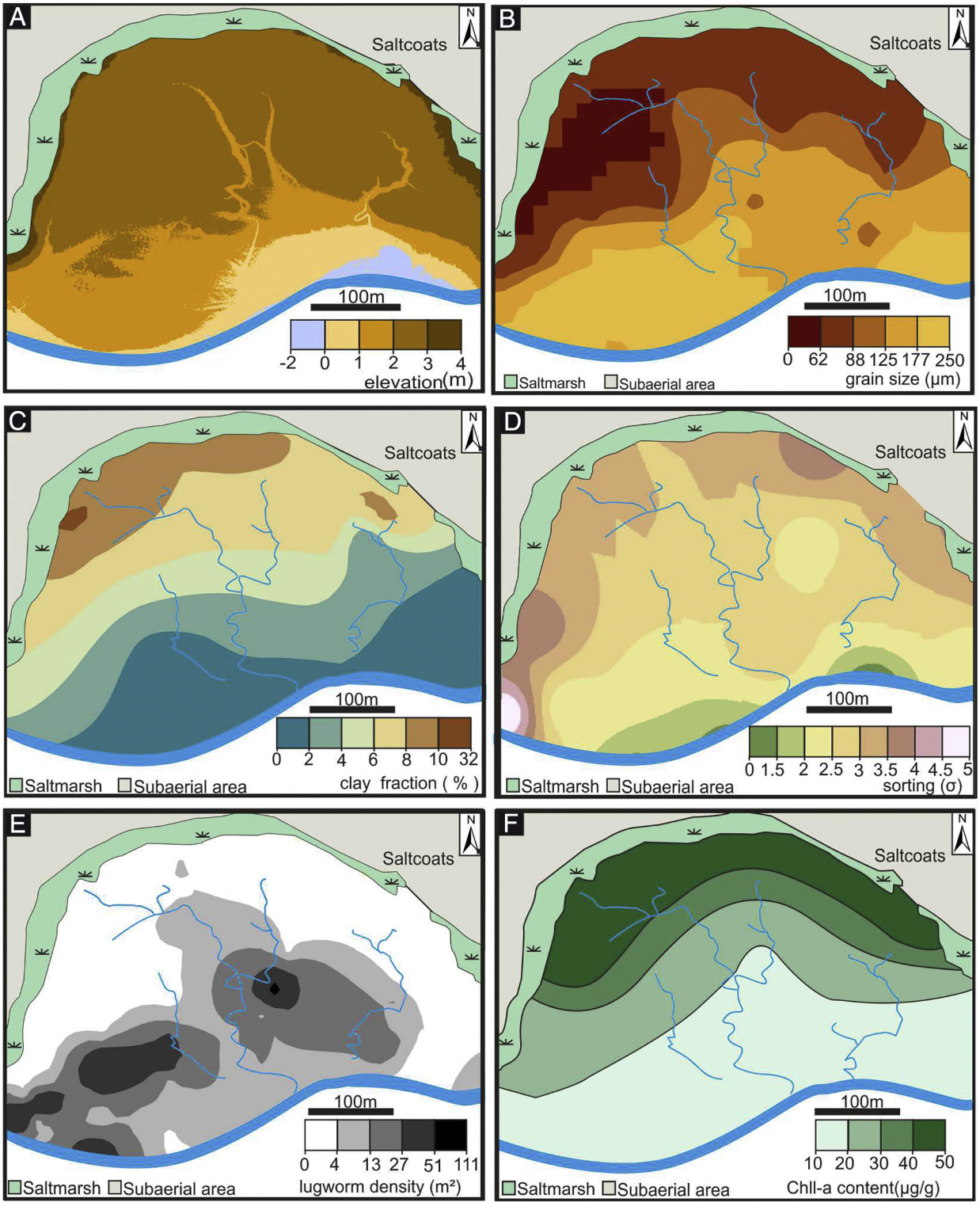
A
Saltcoats
N
100m
-2 0 1 2 3 4
elevation(m)
B
Saltcoats
N
100m
0 62 88 125 177 250
grain size (μm)
Saltmarsh
Subaerial area
C
Saltcoats
N
100m
0 2 4 6 8 10 32
clay fraction (%)
Saltmarsh
Subaerial area
D
Saltcoats
N
100m
0 1.5 2 2.5 3 3.5 4 4.5 5
sorting (σ)
Saltmarsh
Subaerial area
E
Saltcoats
N
100m
0 4 13 27 51 111
lugworm density (m²)
Saltmarsh
Subaerial area
F
Saltcoats
N
100m
10 20 30 40 50
Chll-a content(μg/g)
Saltmarsh
Subaerial area

Figure 4

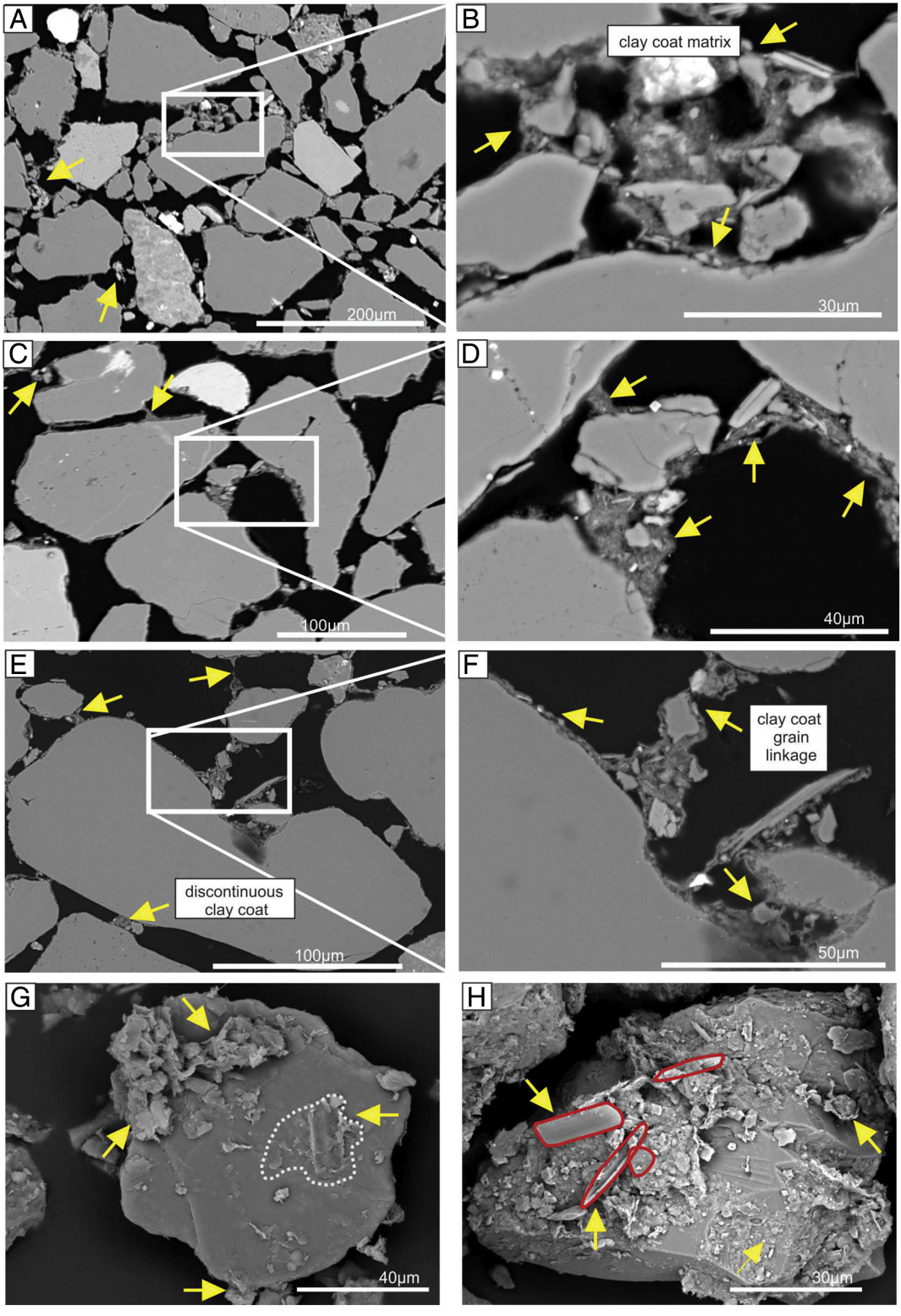
A
200µm
B
clay coat matrix
30µm
C
100µm
D
40µm
E
discontinuous clay coat
100µm
F
clay coat grain linkage
50µm
G
40µm
H
30µm

Figure 5

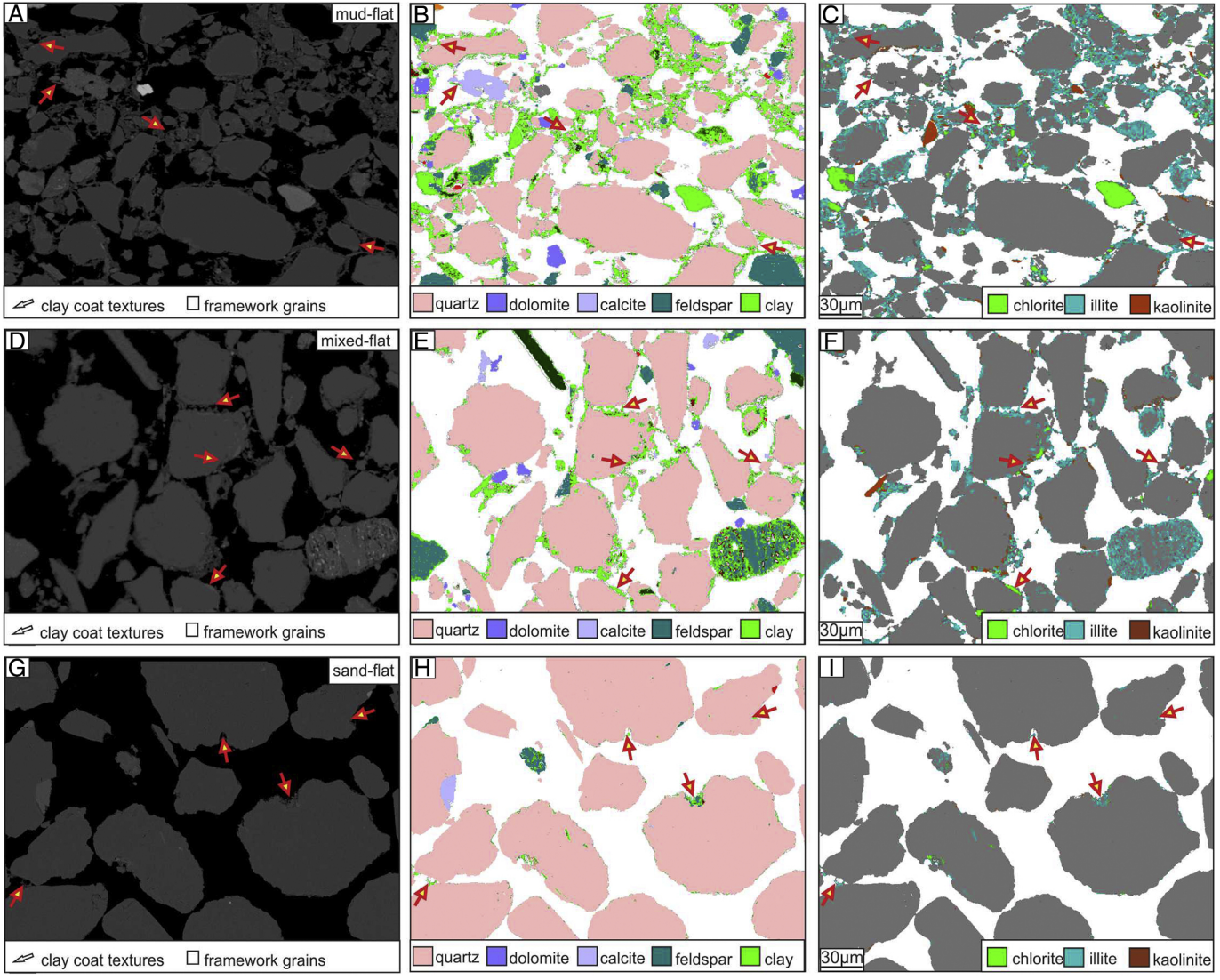
A
mud-flat
clay coat textures
framework grains
B
quartz
dolomite
calcite
feldspar
clay
C
30μm
chlorite
illite
kaolinite
D
mixed-flat
clay coat textures
framework grains
E
quartz
dolomite
calcite
feldspar
clay
F
30μm
chlorite
illite
kaolinite
G
sand-flat
clay coat textures
framework grains
H
quartz
dolomite
calcite
feldspar
clay
I
30μm
chlorite
illite
kaolinite

Figure 6

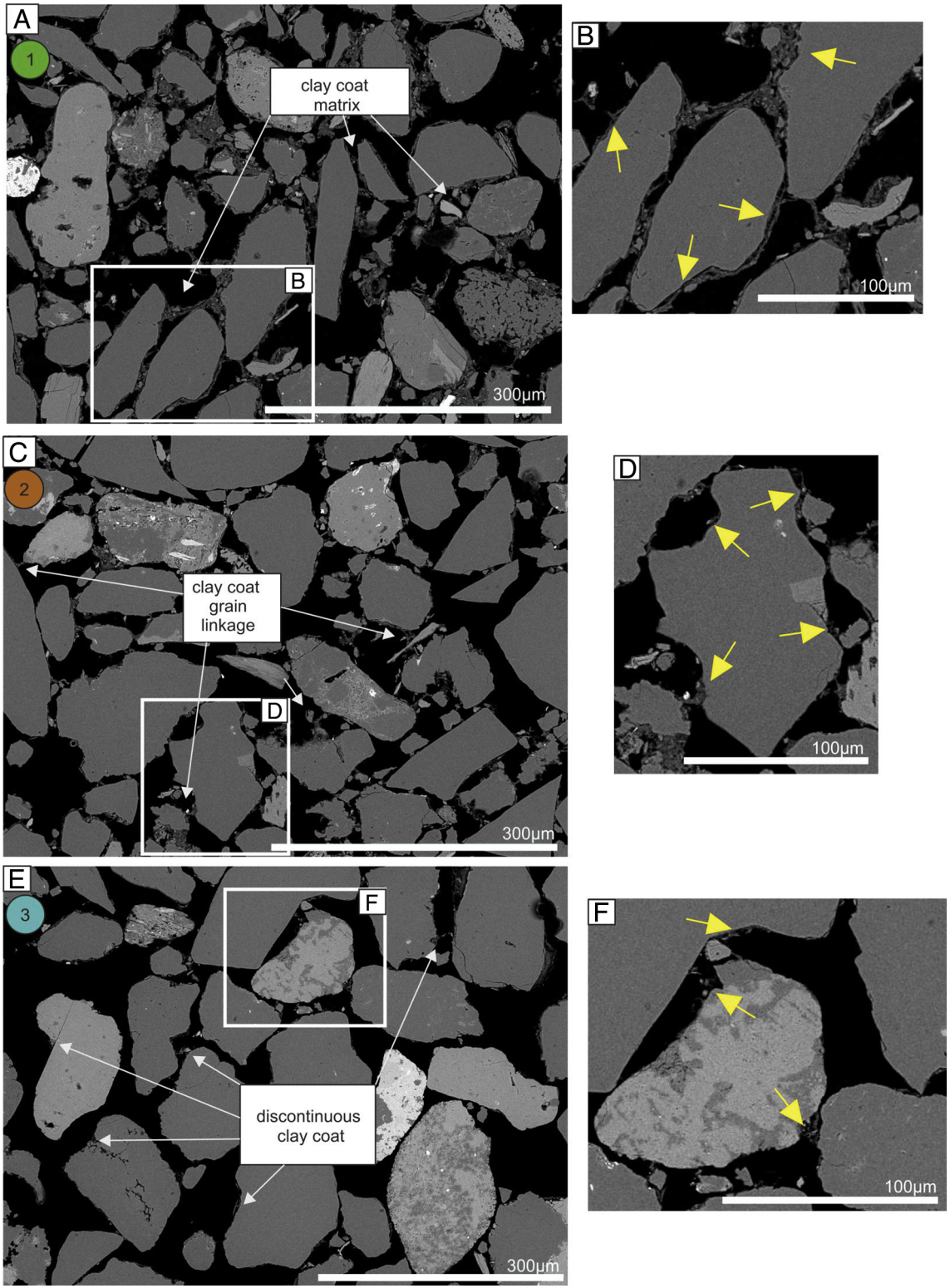
A
1
clay coat
matrix
B
300µm
B
100µm
C
2
clay coat
grain
linkage
D
300µm
D
100µm
E
3
F
discontinuous
clay coat
300µm
F
100µm

Figure 7

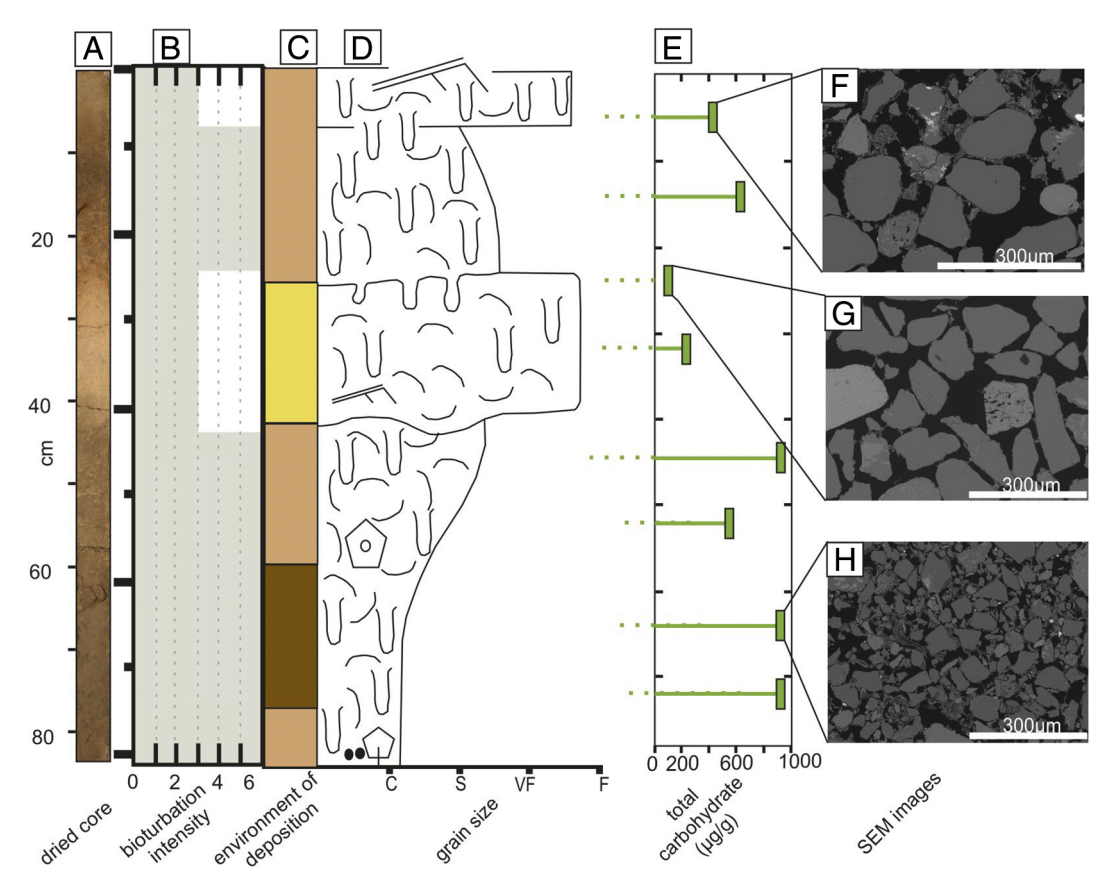
A
B
C
D
E
F
G
H
20
40
cm
60
80
0
2
4
6
dried core
bioturbation intensity
environment of deposition
C
S
VF
F
grain size
0
200
600
1000
total carbohydrate (µg/g)
300um
300um
300um
SEM images

Figure 8

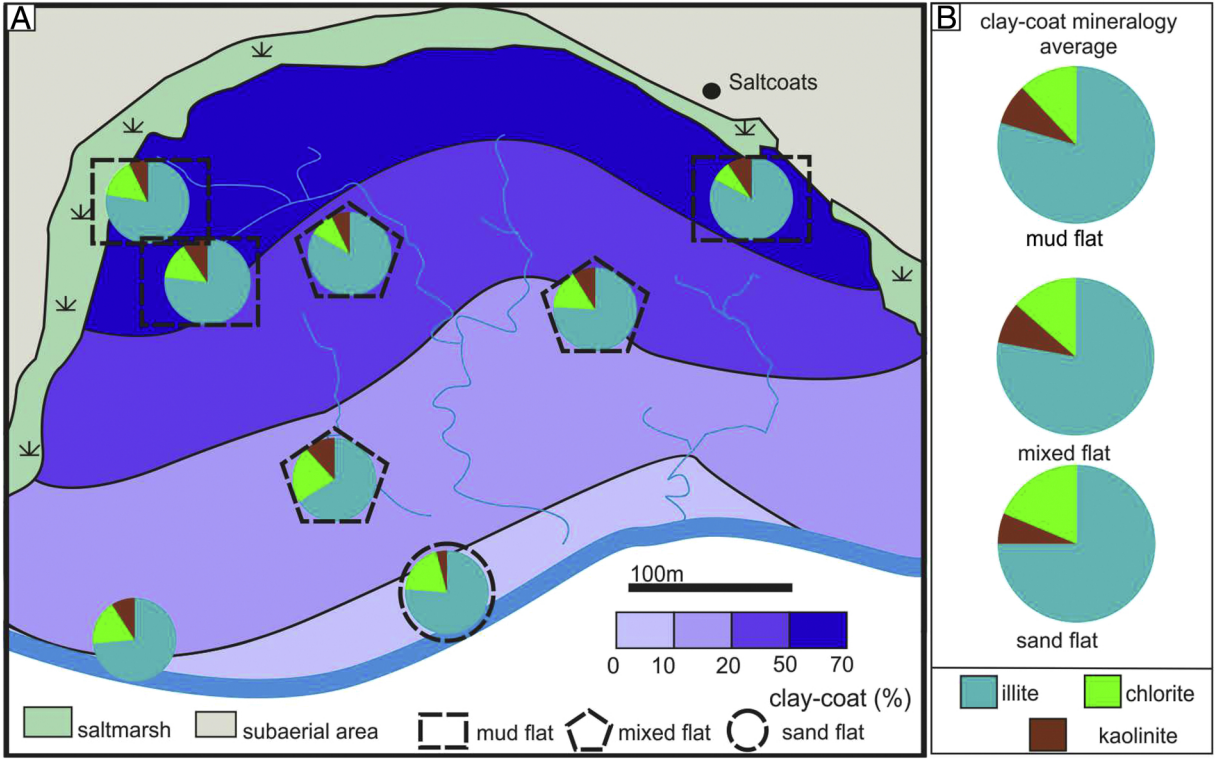
A
Saltcoats
100m
0 10 20 50 70
clay-coat (%)
saltmarsh
subaerial area
mud flat
mixed flat
sand flat
B
clay-coat mineralogy
average
mud flat
mixed flat
sand flat
illite
chlorite
kaolinite

Figure 9

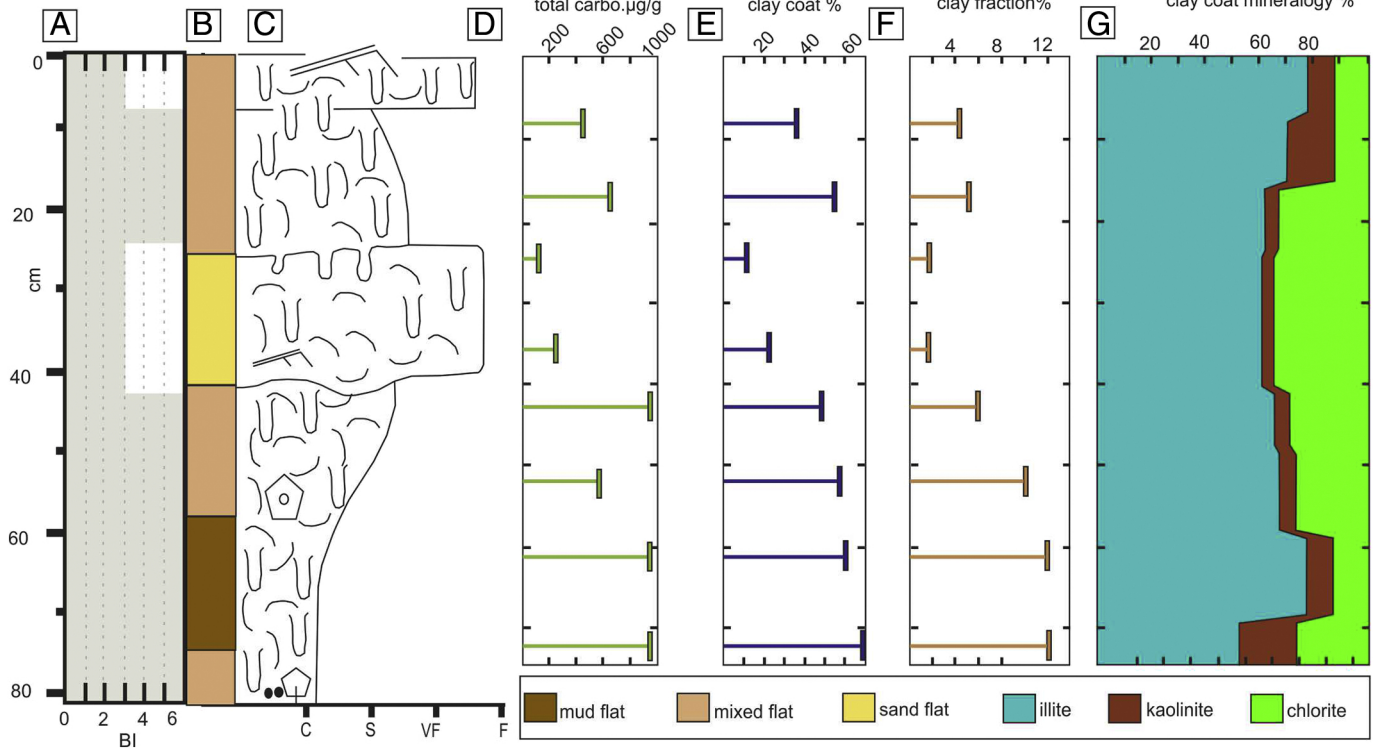
A
B
C
D
E
F
G
0
20
40
60
80
cm
0 2 4 6
BI
C S VF F
total carbo.µg/g
200 600 1000
clay coat %
20 40 60
clay fraction%
4 8 12
clay coat mineralogy %
20 40 60 80
mud flat
mixed flat
sand flat
illite
kaolinite
chlorite

Figure 10

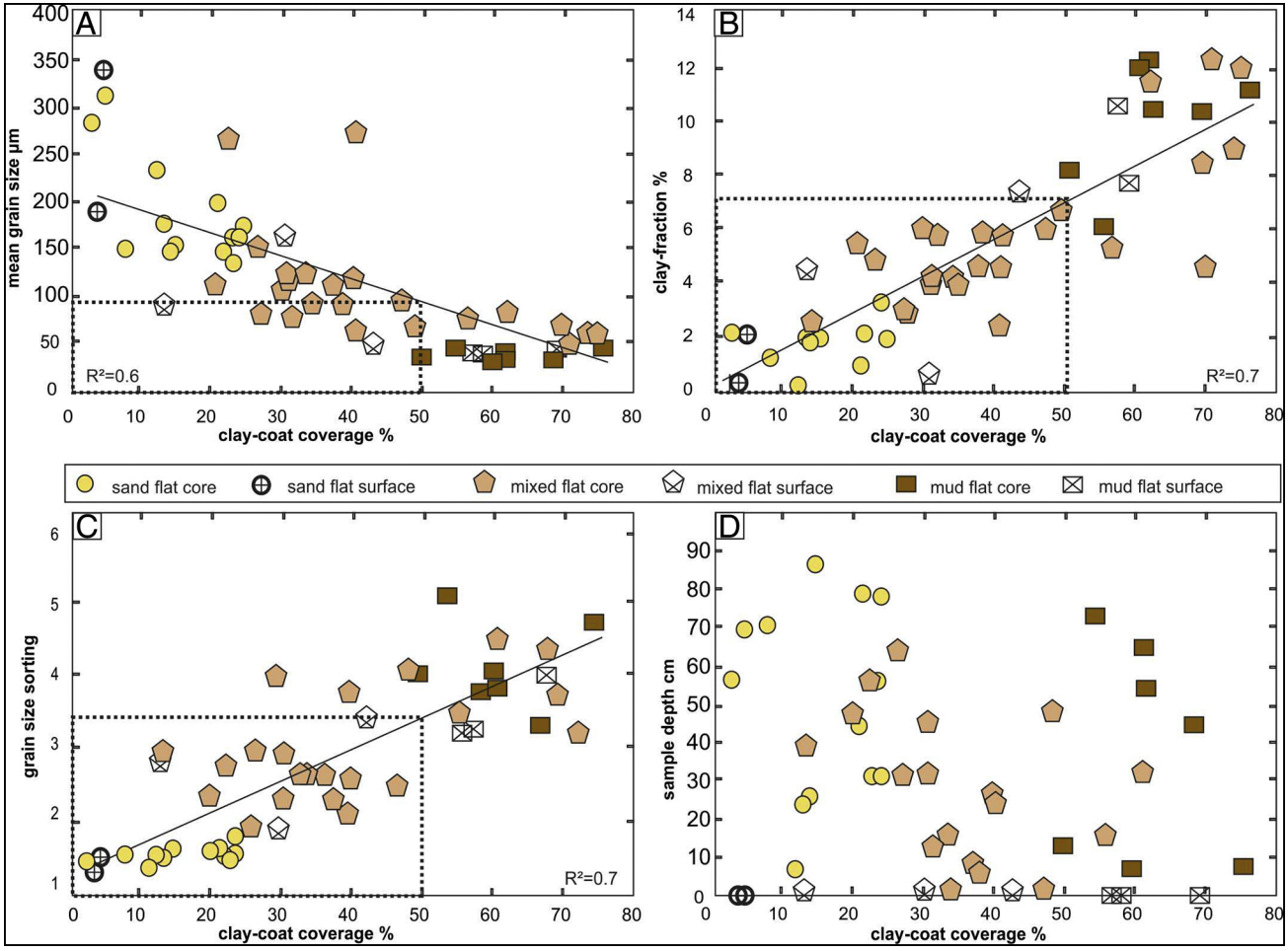
A
mean grain size µm
clay-coat coverage %
R²=0.6
B
clay-fraction %
clay-coat coverage %
R²=0.7
sand flat core
sand flat surface
mixed flat core
mixed flat surface
mud flat core
mud flat surface
C
grain size sorting
clay-coat coverage %
R²=0.7
D
sample depth cm
clay-coat coverage %

Figure 11

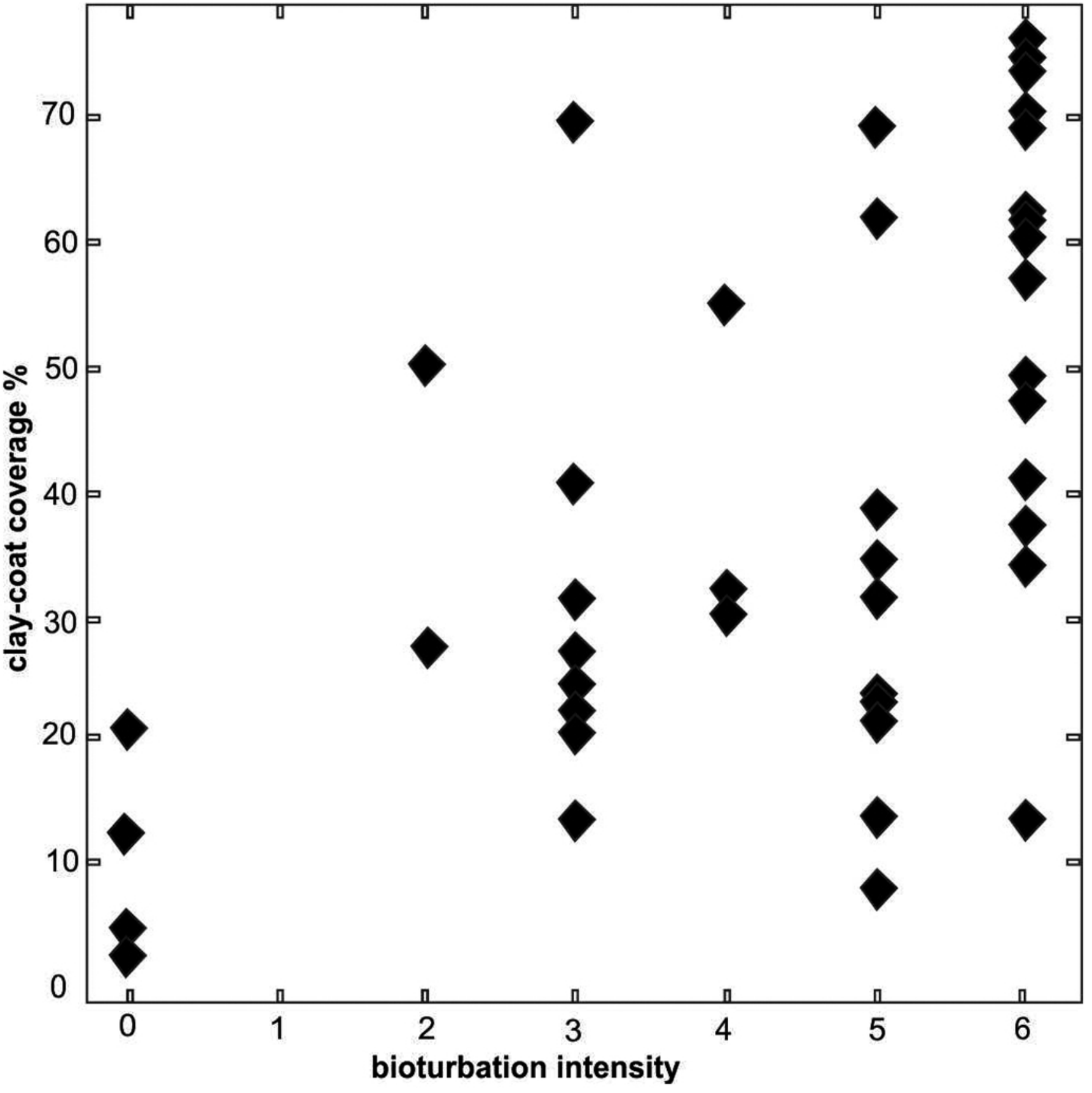
clay-coat coverage %
0
10
20
30
40
50
60
70
0
1
2
3
4
5
6
bioturbation intensity

Figure 12

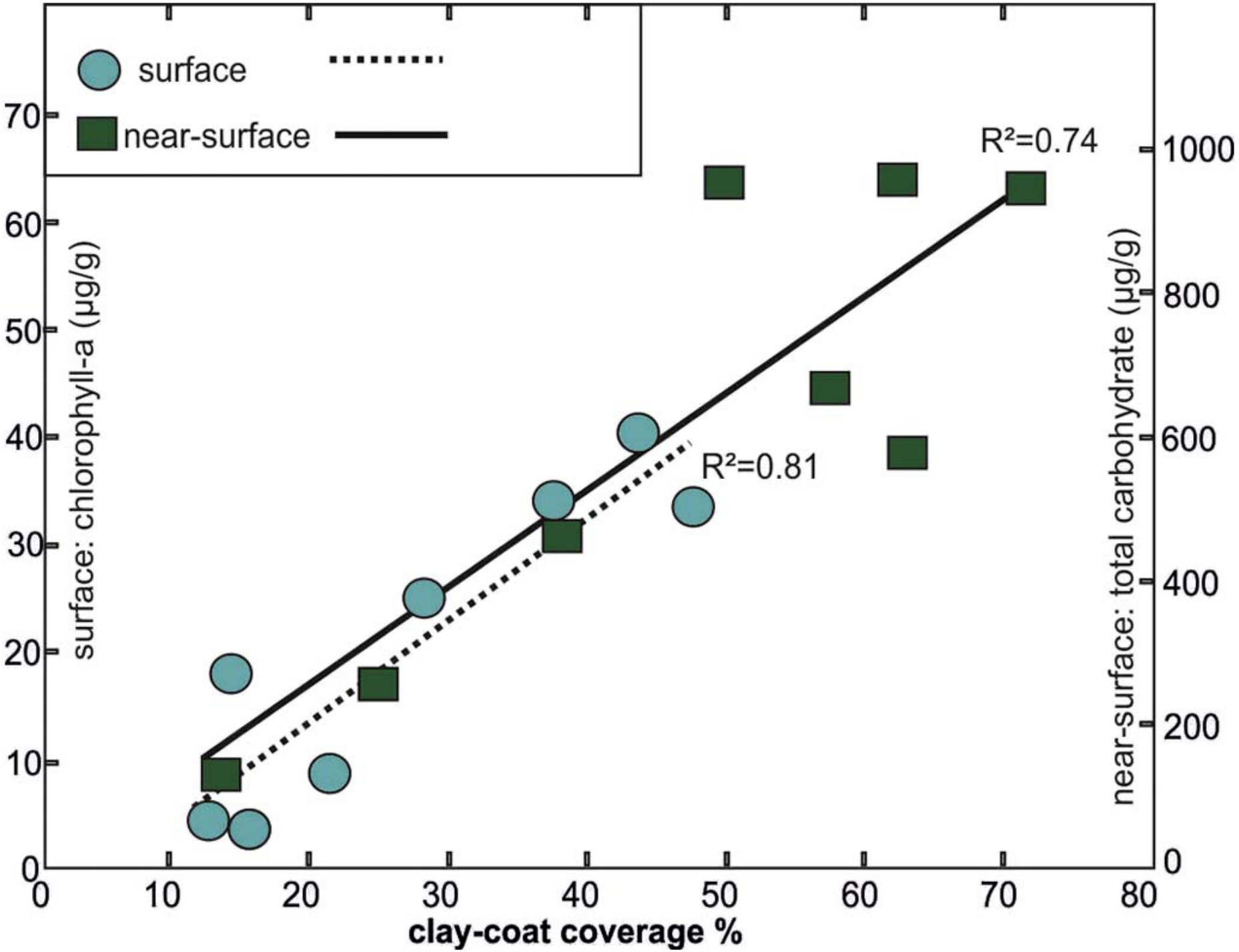
surface
near-surface
R²=0.74
R²=0.81
surface: chlorophyll-a (µg/g)
near-surface: total carbohydrate (µg/g)
clay-coat coverage %
0
10
20
30
40
50
60
70
80
0
200
400
600
800
1000

Figure 13